Ultrasonics Sonochemistry 118 (2025) 107370

Contents lists available at ScienceDirect

Ultrasonics Sonochemistry

journal homepage: www.elsevier.com/locate/ultson

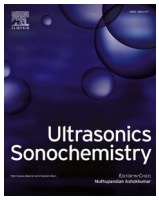

Simultaneous extraction of caffeic acid and production of cellulose microfibrils from coffee grounds using hydrodynamic cavitation in a Venturi tube

Hitoshi Soyama [a,*], Kousuke Hiromori [b], Naomi Shibasaki-Kitakawa [b]

[a] Department of Finemechanics, Tohoku University, 6-6-01 Aramaki, Aoba-ku, Sendai 980-8579, Japan
[b] Department of Chemical Engineering, Tohoku University, 6-6-07 Aramaki, Aoba-ku, Sendai 980-8579, Japan

ARTICLE INFO

Keywords:
Hydrodynamic cavitation
Cellulose microfibril
Caffeic acid
Biomass
Coffee grounds

ABSTRACT

Large quantities of spent coffee grounds (SCGs) are produced daily across the globe, accumulating as industrial waste in factories. Developing a process that both extracts high-value components and utilizes the bulk material would offer significant academic and industrial advantages. This study explores the use of hydrodynamic cavitation, which utilizes the chemical and physical effects produced by bubble collapse, for high-efficiency, continuous processing. The optimization of cavitation conditions was conducted by measuring the aggressive intensity of hydrodynamic cavitation within a Venturi tube. Then, unbrewed coffee grounds was processed by hydrodynamic cavitation to obtain stable results, as caffeic acid in SCGs varied depending on how the coffee was brewed. It was revealed that the hydrodynamic cavitation in the Venturi tube increased extraction rate of coffeic acid and simultaneously generates cellulose microfibrils. Note that the upstream pressure of the Venturi tube was 3.4 MPa, which was generated by a screw pump, and the aggressive intensity of the hydrodynamic cavitation was enhanced by optimizing the downstream pressure of the Venturi tube. The type of cavitation, closely linked to the aggressive intensity, was also analyzed through high-speed photography.

1. Introduction

According to a report by the International Coffee Organization, global coffee consumption is projected to reach approximately 171.3 million 60 kg bags in the 2022/2023 period [1]. There is a growing need for sustainable applications of spent coffee grounds (SCGs), which have accumulated as substantial industrial waste [2–4]. Proposals for extracting biologically active substances such as polyphenols [5–8] and producing biofuel [9] have been put forward, although the primary constituents of SCGs remain largely untapped as waste. Additionally, while methods to enhance the biodegradability of SCGs have been suggested [10], the overall cost of SCG treatment needs consideration. Caffeic acid, which can be extracted from SCGs, has potential applications in cancer treatment [11–17] and the conversion of SCG's main composition into nanofibers or microfibrils for industrial use suggests a sustainable and valuable process, transforming a vast amount of waste into useful industrial materials that produce valuable agents.

Cavitation bubble collapse generates significant physical impacts [18] and chemical effects, including high-temperature and high-pressure zones [19]. These cavitation effects can improve the fatigue strength of metallic materials [20–22] and have been explored for extracting high-value ingredients from renewable biomass [23]. Hydrodynamic cavitation, known for its utility in water treatment [24–29], also shows promise in applications ranging from selective removal of pathogens like Escherichia coli and daphnia [30] to food processing [31], treatment of food wastes [32], wastewater management [24,33,34]. Moreover, it facilitates the degradation of harmful chemicals such as bisphenol A [35,36] and estrogen [37], and aids in the removal of contaminants like succinic acid [38], and dyes [39,40]. Additionally, hydrodynamic cavitation is beneficial in the degradation of ammonia nitrogen [41], biofouling removal [42], synthesis of methyl esters [43,44], and production of ethanol and xylitol [45], among other applications. It is also utilized in oxygen injection [46], preparation of magnesium hydroxide [47], intensification of biogas production [48,49], biodiesel generation [50–53], production of nanoparticles [54], extraction of soybean proteins [55], lemon pectin [56], and proteins and carbohydrates from macroalgae [57], as well as in the pretreatment of biomass [58–73].

* Corresponding author.
E-mail address: soyama@mm.mech.tohoku.ac.jp (H. Soyama).

https://doi.org/10.1016/j.ultsonch.2025.107370
Received 7 February 2025; Received in revised form 1 April 2025; Accepted 22 April 2025
Available online 23 April 2025

When considering the primary composition of SCGs, they can be transformed into cellulose nanofibers or microfibrils [74–76]. These nanocellulose materials are valuable for developing polymer matrix composites [77,78], high-performance electromagnetic interference (EMI) shielding materials [79], and sustainable active packaging [80]. The mechanical properties of cellulose nanofibers, such as tensile strength, have been extensively studied to facilitate their application in industrial materials [81]. Regarding the production methods, techniques like ultrasonication [82–86] and microfluidic device-based cavitation [87] have been proposed. Notably, the pretreatment efficiency of hydrodynamic cavitation has been reported to be 20 times more effective than ultrasonic cavitation [58], suggesting that further exploration of cellulose nanofiber and microfibril production via hydrodynamic cavitation is warranted.

In terms of generating hydrodynamic cavitation for chemical reactors [88], various configurations have been explored, including cavitating jets [89], Venturi tubes [58,90], orifice plates [91,92], jet pumps [93,94], swirling vortex flows [95–97], rotor-radial grooves [98], and rotor–stator designs [52]. It has been observed that vortex cavitation in a Venturi tube is particularly effective, strongly correlated with the aggressive intensity of hydrodynamic cavitation [99]. This study focuses on the application of hydrodynamic cavitation within a Venturi tube, examining its efficiency in detail. The relationship between cavitation types—such as spherical bubbles, swirling, tip, and turbulent vortex cavitation—and the aggressive intensity of cavitation collapse is crucial, as the turbulent eddies in the Venturi tube intensify the cavitation collapse [100]. While the extraction of bioactive substances like caffeic acid from SCGs is promising, the sustainability of the process is challenged by the large volume of residue generated. However, converting this residue into industrially valuable materials like cellulose nanofibers or microfibrils could render the process both economically and environmentally beneficial.

In this study, a method for extracting caffeic acid from unbrewed coffee grounds using hydrodynamic cavitation in a Venturi tube was investigated, aiming for more consistent results while concurrently converting the residue into cellulose microfibrils. The simultaneous extraction of caffeic acid and production of cellulose microfibrils were validated experimentally. As the aggressive intensity of cavitation varies with the type of cavitation as mentioned above, the aspect of hydrodynamic cavitation was observed by high speed photography.

2. Materials and methods

2.1. Materials

To achieve a more stable extraction rate of caffeic acid from coffee grounds, unbrewed coffee grounds were selected due to the variability in caffeic acid content in SCGs based on the brewing method. The coffee grounds used were from a consistent lot of commercially available paper filter drip coffee (Home Brewed Product Series, Kilimanjaro Blend, KEY COFFEE INC, Tokyo, Japan). These grounds were pulverized in a blender and sifted through a wire mesh with a 355 μm aperture. In the extraction process, 15 g of coffee grounds were mixed into 3 L of a 30 vol % ethanol aqueous solution. This particular concentration of ethanol was chosen because it effectively dissolves caffeic acid while aligning with the requirements for managing the aggressive intensity of the hydrodynamic cavitation. The aggressive intensity was evaluated by measuring the luminescence intensity generated by hydrodynamic cavitation in a Venturi tube, as noted in a previous study [99] and by evaluating the cavitation erosion rate using a cavitating jet apparatus [101]. The experimental setup involved an injection pressure of 0.5 MPa for luminescence intensity measurements and 10 MPa for cavitation erosion testing. The main findings, illustrating the variation of the luminescence intensity and cavitation erosion rate with the ethanol concentration, are detailed in Appendices A and B. Both the low and high injection pressure tests showed peak aggressive intensities at a 30 vol% ethanol concentration, which was subsequently used in the experiments.

2.2. Hydrodynamic cavitation apparatus using Venturi tube

Figs. 1 and 2 provide a schematic of hydrodynamic cavitation using a Venturi tube and detail its geometric specifications. The throat diameter of the Venturi tube measures 0.7 mm. Both the inlet and outlet angles are set at 20°, as depicted in Fig. 2. The tube is constructed from brass for operational durability and acrylic resin to facilitate observation of the cavitation process. A 30 vol% ethanol aqueous solution containing coffee grounds is loaded into a hopper-type tank, which holds up to 6.6 L and has a maximum diameter of 210 mm. This solution is pressurized by a screw pump capable of reaching a maximum pressure of 3.6 MPa and a flow rate of 3.8 L/min. The tank and pump are interconnected using a stainless steel pipe with an inner diameter of 35 mm, while the connecting pipes for the pump, valves, and Venturi tube have an inner diameter of 8 mm. During the cavitation process, a bypass valve is closed to ensure the solution is pressurized by the pump and directed into the Venturi tube. The upstream pressure of the Venturi tube, denoted as p_1, is regulated by adjusting the pump's rotational speed. Conversely, the downstream pressure (p_2) is modified by manipulating the downstream valve. Both upstream and downstream pressures are monitored using pressure gauges. In the control process, the downstream valve is closed, allowing the pressurized solution to be recirculated back into the tank via a bypass pipe with an 8 mm inner diameter. The pump's rotational speed during the control process is maintained at the same level as during the cavitation condition.

The cavitation number, σ, a critical parameter in cavitating flows [18], is defined by Eq. (1), as p_1 and p_2 were described as gauge pressures in MPa.

$$\sigma = \frac{(p_2 + 0.1) - p_v}{(p_1 + 0.1) - (p_2 + 0.1)} = \frac{(p_2 + 0.1) - p_v}{p_1 - p_2}, \tag{1}$$

where p_v is the vapor pressure of the liquid. In this study, p_v was calculated from the vapor pressures of water and ethanol considering the concentration ratio of ethanol. During the process, the solution temperature was kept at 293 ± 2 K by an immersion type chiller.

2.3. Evaluation of aggressive intensity of hydrodynamic cavitation

It has been observed that the aggressive intensities of acoustic noise and luminescence generated by hydrodynamic cavitation in the Venturi tube vary with p_1 and p_2 [99,102]. These aggressive intensities were measured using a sound level meter, which can assess cavitation noise [103]. The meter was positioned perpendicular to the Venturi tube, at a

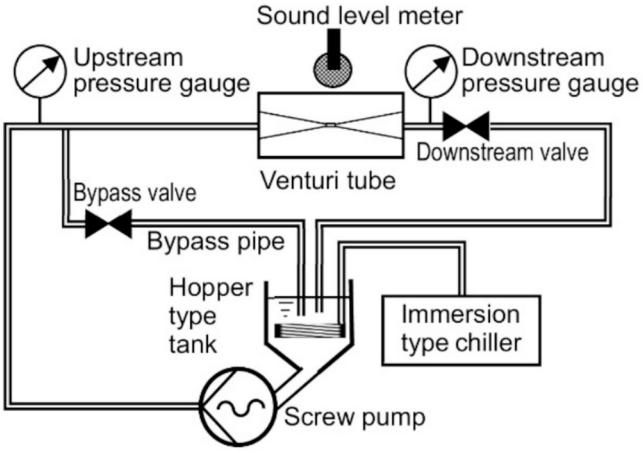

Fig. 1. Schematic diagram of experimental setup.

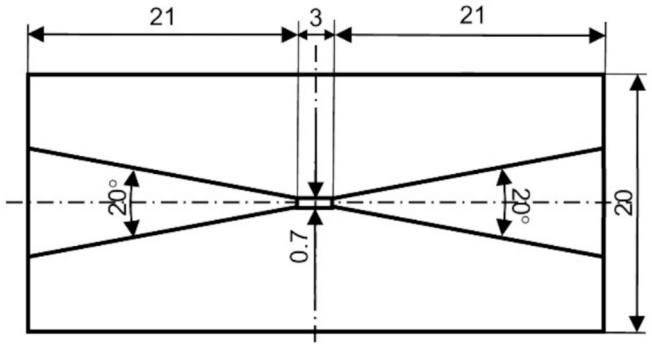

Fig. 2. Schematic of the Venturi tube (unit: mm).

distance of 50 mm. For the measurement, Z-weighted sound levels, which remain flat from 10 Hz to 20 kHz, were employed. The noise level (N_L) was recorded as an average over 10 s and expressed in decibels (dB). Since the acoustic intensity is proportional to the square of the acoustic pressure (p_a) [103], the aggressive intensity of cavitation (I_{cav}) was defined by Eq. (2), where p_a is derived from the N_L.

$$I_{cav} = \frac{{p_a}^2}{\rho c} = \frac{(20 \times 10^{-6} \times 10^{\frac{N_L}{20}})^2}{\rho c}, \quad (2)$$

where ρ and c denote the density and velocity of sound in the solution, respectively. The pump power P_J [kW] for upstream pressure p_1 [MPa] and flow rate Q [L/min] are defined by Eq. (3), the treatment efficiency of coffee grounds using cavitation was considered. Note that Q, which varied with p_2 at constant p_1 of used the Venturi tube, was approximately equivalent as shown in Appendix C.

$$P_J = \frac{1 \times 10^6 \times p_1 \times Q}{60\eta}, \quad (3)$$

where η is efficiency of the pump.

The aggressive intensity of cavitation, closely linked to bubble geometry [100], was meticulously observed using a high-speed video camera capable of capturing up to 8,000 frames per second (fps) in full frame (1,600 × 1,200 pixels) and up to 194,000 fps in partial frame (1,600 × 16 pixels). Additionally, a digital camera with a resolution of 5,568 × 3,712 pixels, equipped with a flash lamp, was used to capture detailed images. The flash lamp's exposure time was set to 1.5 μs. Both high-speed video and digital cameras were positioned perpendicularly to the Venturi tube. To enhance the visibility of the cavitation process, observations from two different angles were facilitated using a mirror, as depicted in Fig. 3.

2.4. Characterization of treated coffee grounds

To demonstrate the production of microfibrils from coffee grounds, the solution and sediment were freeze-dried and examined under a scanning electron microscope (SEM).

The concentration of extracted caffeic acid was determined using high-performance liquid chromatography (HPLC) system equipped with an ultraviolet detector (Waters Corp. Milford, MA. USA, ACQUITY UPLC H-Class System) and an ACQUITY UPLC BEH C18 column (Waters Corp., particle size 1.7 μm, i.d. 2.1 mm, length150 mm). Acetonitrile (Wako Pure Chemical Industries, Ltd., Osaka, Japan, HPLC AR Grade), trifluoroacetic acid (Wako Pure Chemical Industries, Ltd., HPLC AR grade), and ultrapure water were used as a mobile phase at a flow rate of 0.6 cm^3/min by a gradient elution. The temperature of the column oven was 40 °C and the detection wavelength was 325 nm. In this study, the extraction rate was quantified relative to the benchmark extraction rate of caffeic acid using the Soxhlet extraction method.

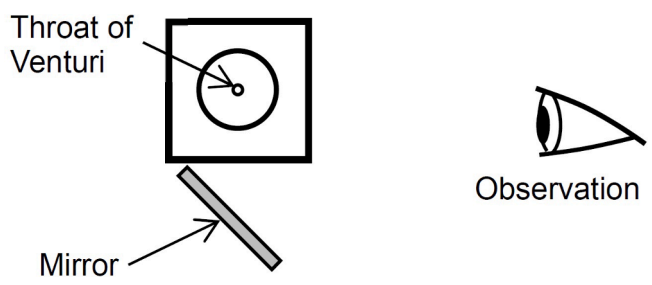

Fig. 3. Diagram showing the direction of observation.

3. Results

3.1. Aggressive intensity of hydrodynamic cavitation in Venturi tube

Fig. 4 shows the noise level N_L of the cavitation noise generated by the hydrodynamic cavitation of 30 vol% ethanol aqueous solution measured by the sound level meter as a function of p_2 at p_1 = 1.4, 1.9, 2.4, 2.9 and 3.4 MPa. As the sound level was measured three times at each condition, the plot in Fig. 4 shows mean value and error bar reveals standard deviation. The noise level N_L owing to the hydrodynamic cavitation of water at p_1 = 3.4 MPa is shown in Fig. 4. All N_L values increased with increasing p_2, peaked, and then decreased. As discussed in section "*3.2. Aspect of hydrodynamic cavitation in Venturi tube*", the cavitating region decreased monotonically with an increase in p_2, however, N_L had a peak with respect to p_2. This behavior of N_L is consistent with patterns observed in acoustic energy [102] and luminescence intensity [99,102]. Notably, measuring N_L with a sound level meter is considerably simpler than measuring acoustic energy via pulse height analysis [102] or luminescence intensity, as it does not require specialized equipment.

To clarify the mechanism behind the peak in N_L against p_2, Fig. 5 illustrates N_L as a function of the cavitation number σ. The plot and error bar in Fig. 5 show mean value and standard deviation as same as Fig. 4. As shown in Fig. 4, p_2 at which N_L had the maximum value, i.e., N_{Lmax}, increased with p_1. For example, p_2 at which N_L had maximum, $p_{2\ max}$, was 0.152 MPa for p_1 = 1.4 MPa, 0.178 MPa for p_1 = 1.9 MPa, 0.209 MPa for p_1 = 2.4 MPa, 0.224 MPa for p_1 = 2.9 MPa, and 0.28 MPa for p_1 = 3.4 MPa. On the other hand, the peak N_L occurred at σ = 0.12 – 0.16 for p_1 = 1.9, 2.4, 2.9 and 3.4 MPa. This suggests that the tendency of N_L to vary with p_2 is a characteristic of a cavitating flow, similar to the main parameter σ. It has been demonstrated that the aggressive intensity of

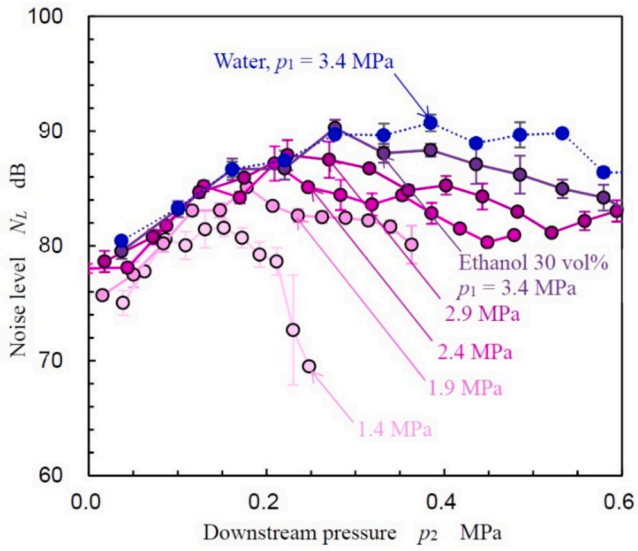

Fig. 4. Variation in noise level (N_L) with downstream pressure (p_2).

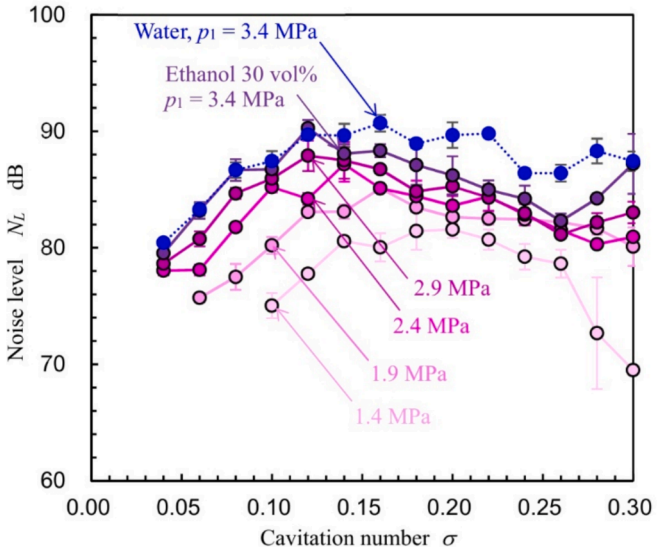

Fig. 5. Noise level (N_L) as a function of the cavitation number (σ).

hydrodynamic cavitation in a Venturi tube is estimated by the sound velocity, frequency of vortex cavitation, and cavitating length [99]. Although the cavitation length decreases with p_2, the sound velocity, which increases the individual cavitation bubble collapse, increases with p_2 under a constant p_1 condition [99].

To explore process efficiency improvements by optimizing p_2, Fig. 6 depicts the normalized aggressive intensity I_{cav}' of hydrodynamic cavitation in the Venturi tube as a function of injection pressure p_1. As Q at constat p_1 was approximately equivalent as shown in Fig. C1 (Appendix C), P_J was proportional to p_1, then Fig. 6 reveals I_{cav}' as a function of p_1. In Fig. 6, the aggressive intensity I_{cav}, which was defined by Eq. (2), was normalized by I_{cav} at p_1 = 1.4 MPa and p_2 = 0.06 MPa. As shown in Fig. 5, N_L at $p_2 \approx 0$ MPa and $p_2 = p_{2\,max}$ were increased with p_1. Thus, I_{cav}' at $p_2 \approx 0$ MPa and I_{cav}' at $p_2 = p_{2\,max}$ were increased. In Fig. 6, the luminescence intensity I_L [99] at $p_2 = p_{2\,max}$ was also revealed. I_L was

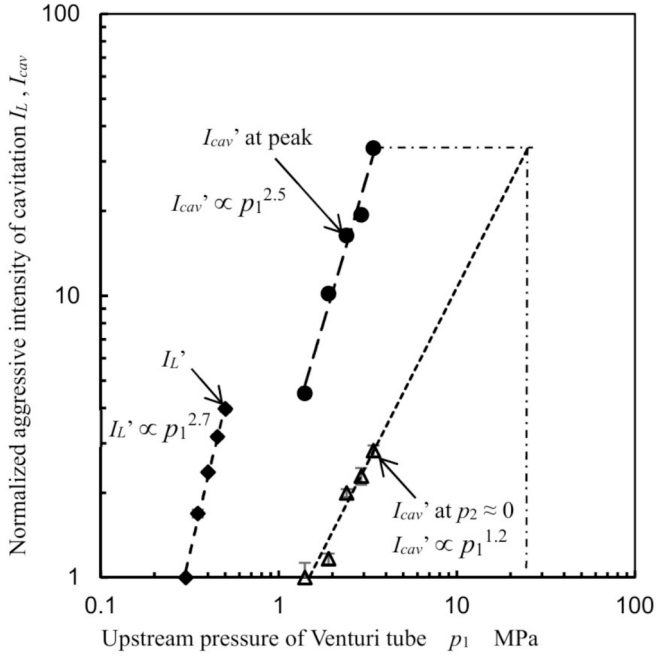

Fig. 6. Variation in aggressive intensity of cavitation with upstream pressure in the Venturi tube.

normalized to I_L at p_1 = 0.3 MPa. Assuming a power law relationship for the variation of I_{cav}' and I_L' with p_1, the following equations were derived.

$$I'_{cav} \propto p_1^{1.2}, \quad (p_2 \approx 0\,\text{MPa}), \tag{4}$$

$$I'_{cav} \propto p_1^{2.5}, (p_2 = p_{2max}), \tag{5}$$

$$I'_{L} \propto p_1^{2.7}, (p_2 = p_{2max}). \tag{6}$$

As shown in Eqs. (4) – (6), the exponents at $p_2 = p_{2\,max}$ are larger than those at $p_2 \approx 0$ MPa. Moreover, the value 2.5 from Eq. (5) closely approximates the 2.7 in Eq. (6). Fig. 6 demonstrates that I_{cav}' at p_1 = 3.4 MPa and $p_2 = p_{2\,max}$ is 7.4 times greater than that at p_1 = 3.4 MPa and $p_2 \approx 0$. Assuming extrapolation as per Eq. (4), I_{cav}' at p_1 = 3.4 MPa and $p_2 = p_{2\,max}$ equates to I_{cav}' at p_1 = 25 MPa and $p_2 \approx 0$ MPa. According to Eq. (3), the required electrical power for the pump at p_1 = 25 MPa is 20 times greater than at p_1 = 3.4 MPa. Therefore, optimizing p_2 is advantageous for reducing pump power consumption. Reflecting the N_L findings from Figs. 4 and 5, the process conditions for the coffee grounds were set at p_1 = 3.4 MPa and p_2 = 0.28 MPa, where N_L reaches its maximum in a 30 vol% ethanol aqueous solution.

3.2. Aspect of hydrodynamic cavitation in Venturi tube

Fig. 7 depicts changes in hydrodynamic cavitation at p_1 = 3.4 MPa across (a) water and (b) 30 vol% ethanol aqueous solutions, with the flow direction from left to right. The white areas resembling clouds in Fig. 7 indicate the cavitating region. In both (a) water and (b) the ethanol solution, cavitation develops downstream from the throat, and the cavitating length decreases consistently with an increase in p_2. Downstream vortex cavitation, characterized by angulated rather than spherical bubbles, was observed [104]. Despite the reduction in cavitating length from p_2 = 0.04 MPa to p_2 = 0.28 MPa, N_L increased. This increase may be attributed to the intensified individual cavitation collapses due to a decreased void ratio in the cavitation region, compounded by an increased acoustic impedance from higher sound velocities [99]. Comparing cavitation effects between water and the solution, the residual bubbles following cavitation collapse in the solution were notably denser at p_2 = 0.04 MPa, especially evident as the white regions in the solution appeared denser than those in water. The differences between water and the solution diminish with increasing p_2, and the presence of vortex cavitation becomes more pronounced. In summary, the characteristic cavitation in a 30 vol% ethanol aqueous solution at p_1 = 3.4 MPa and p_2 = 0.28 MPa was identified as vortex cavitation, similar to that observed in water.

To examine the structure of vortex cavitation, Figs. 8 and 9 display the cavitation observed from two perspectives using a mirror (refer to Fig. 3), both with and without coffee grounds. The flow directions in Figs. 8 and 9 are consistent with those in Fig. 7. Each of these figures illustrates three typical representations of vortex cavitation at the conditions of p_1 = 3.4 MPa and p_2 = 0.28 MPa. In each image set, the upper photo shows a direct view while the lower photo depicts the mirrored image. Due to the Venturi tube's design, which includes a corner at the throat inlet and outlet, the cavitating region appears slightly skewed, with the top part of the mirrored image exhibiting a longer cavitating region than the bottom part. As clearly demonstrated in Fig. 8 (a), the vortex cavitation located 10 mm from the throat outlet is inclined at a 45° angle relative to the main flow direction resembling the helical vortex structures previously reported [104]. Similarly, Fig. 9 (a), (b), and (c) show that vortex cavitation is also distinctly visible in the hydrodynamic cavitation of the solution.

To further explore how vortex cavitation evolves over time, Fig. 10 presents high-speed video camera footage of hydrodynamic cavitation in a 30 vol% ethanol aqueous solution mixed with coffee grounds at p_1 = 3.4 MPa and p_2 = 0.28 MPa. The recording speed was set at 50,000 fps.

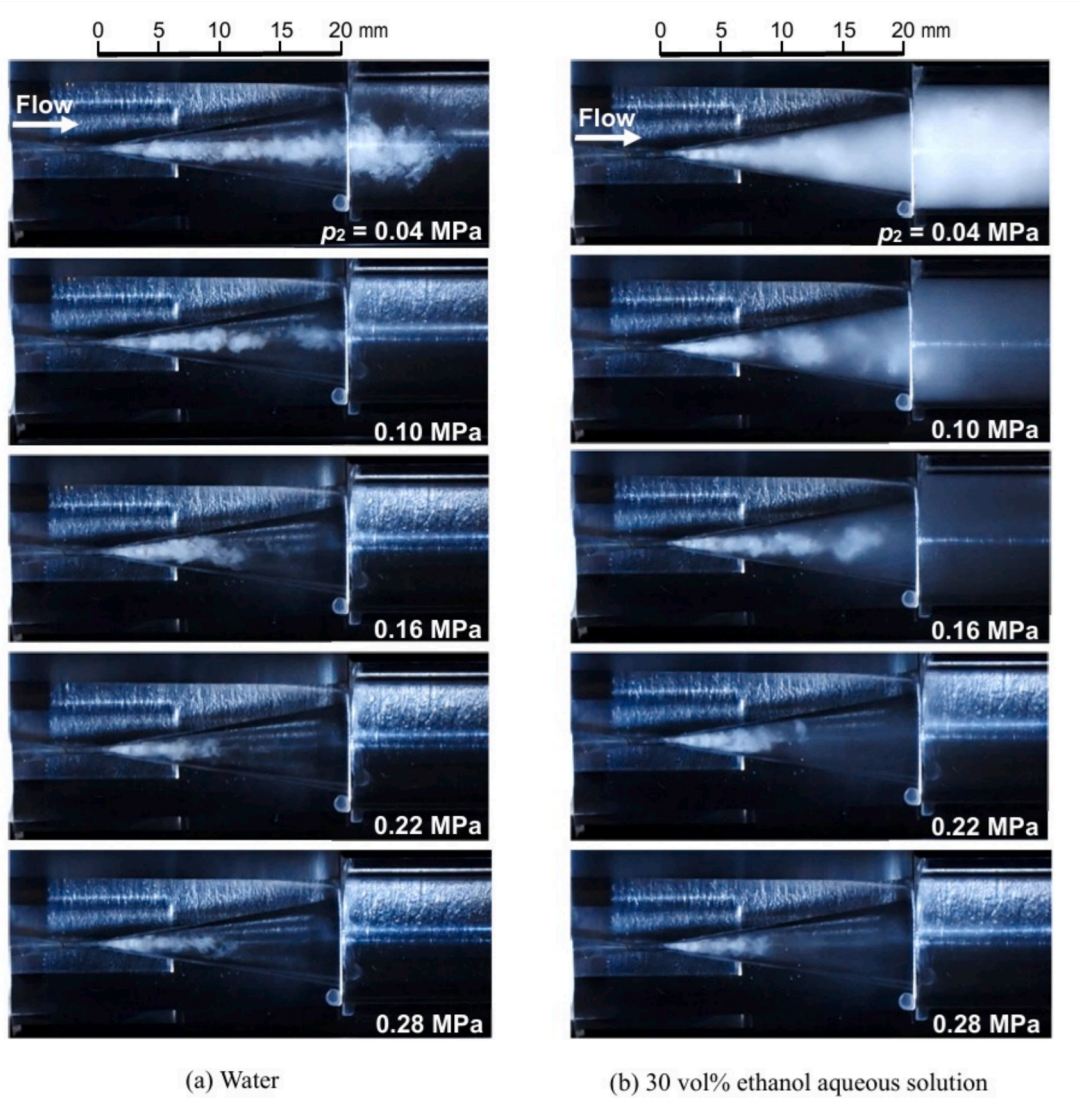

Fig. 7. Visual representation of cavitation dynamics at different downstream pressures (p_2) with upstream pressure p_1 = 3.4 MPa:

In this figure, the flow direction aligns with that in Figs. 7–9. The vortex cavitation, indicated by blue arrows at t = 0.10 ms and t = 0.30 ms, is observed to be angled at 45° to the main flow direction. These vortex cavitations are shed from the trailing edges of the cavitating regions that develop from the throat and subsequently collapse, generating pressure during their collapse [99]. However, under the current conditions, it is very challenging to distinguish coffee grounds using high-speed video cameras.

3.3. Extraction of coffeic acid by hydrodynamic cavitation in Venturi tube

To demonstrate the effectiveness of extracting caffeic acid through hydrodynamic cavitation in a Venturi tube, Fig. 11 presents the relative concentration of caffeic acid (ρ_c') over the processing time (t_p). The ρ_c' was determined by normalizing the caffeic acid concentration of non-treated coffee grounds measured by the Soxhlet extraction method, i.e., 6.544×10^{-5} mol/g. The conditions maintained were a p_1 of 3.4 MPa and a p_2 of 0.28 MPa, utilizing a 30 vol% ethanol aqueous solution. Samples of 15 ml were collected every 30 min. Both "control" and "cavitation" processes were conducted three times to ensure reliability. The circles in Fig. 11 show mean values, and the error bars indicate the standard deviations of three sets of experiments. At t_p = 30 min, ρ_c' was 0.832 ± 0.012 for the control and 0.899 ± 0.014 for the cavitation process. Despite the standard deviation, there was a significant enhancement in extraction efficiency during cavitation. While ρ_c' for the control condition gradually increased and plateaued at 120 min, the cavitation process maintained ρ_c' approximately at 0.9 from 30 to 150 min, indicating that hydrodynamic cavitation under these specific conditions effectively enhanced the extraction of caffeic acid.

3.4. Production of cellulose microfibril by hydrodynamic cavitation in Venturi tube

To illustrate the defibration of coffee grounds, Fig. 12 displays the appearance of 15 mL polystyrene bottles containing (a) the solution with coffee grounds prior to processing, (b) the solution with sediment after undergoing the control process for 150 min, and (c) the solution with sediment after experiencing cavitation for 150 min. Each scenario utilized a 30 vol% ethanol aqueous solution. Behind each bottle, a double-cross sign plate, employed in the transparency test for industrial wastewater according to the Japanese Industrial Standards JIS K0102-2021, was positioned. In the case of (a), 75 mg of coffee grounds were added to a 15 mL solution, maintaining a concentration of 0.5 wt%, consistent with the control and cavitation processes. In cases (b) and (c), after each 150-min process, the solutions were transferred into bottles with almost identical amounts of sediment and were left undisturbed for

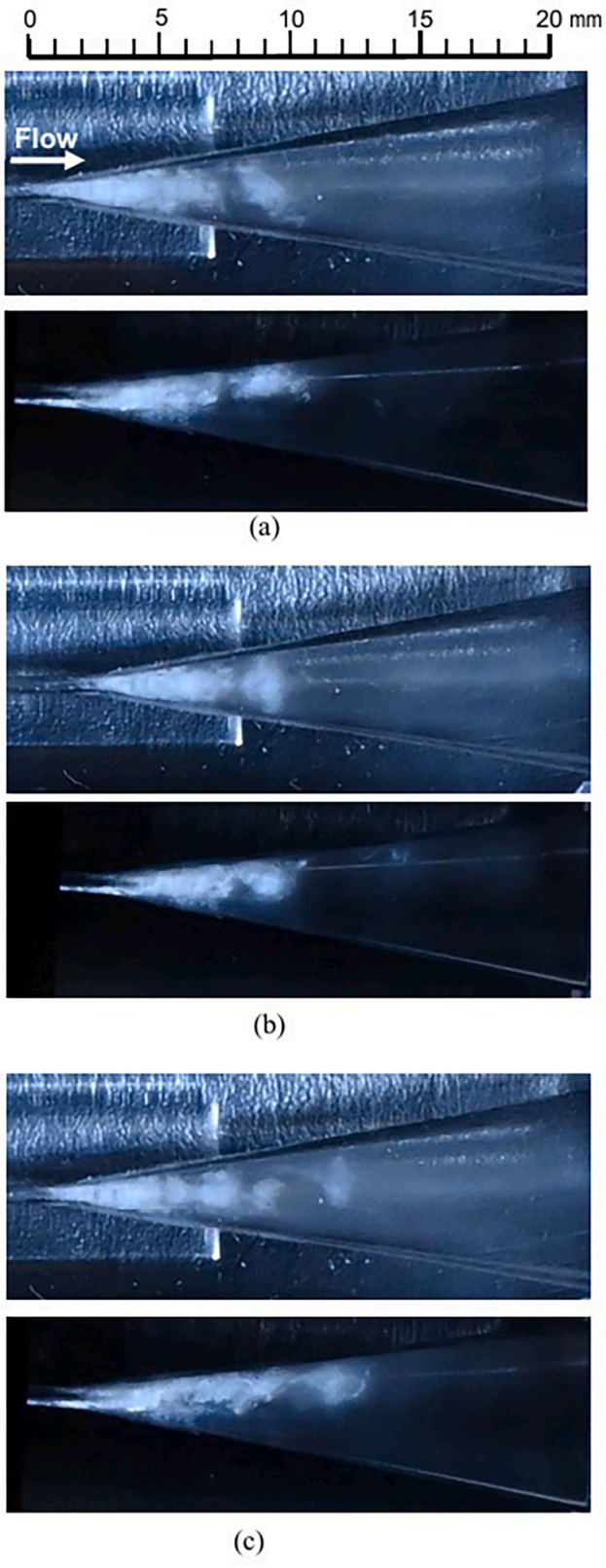

Fig. 8. Visualization of vortex cavitation without coffee grounds observed from two perspectives in a 30 vol% ethanol aqueous solution (p_1 = 3.4 MPa, p_2 = 0.28 MPa).

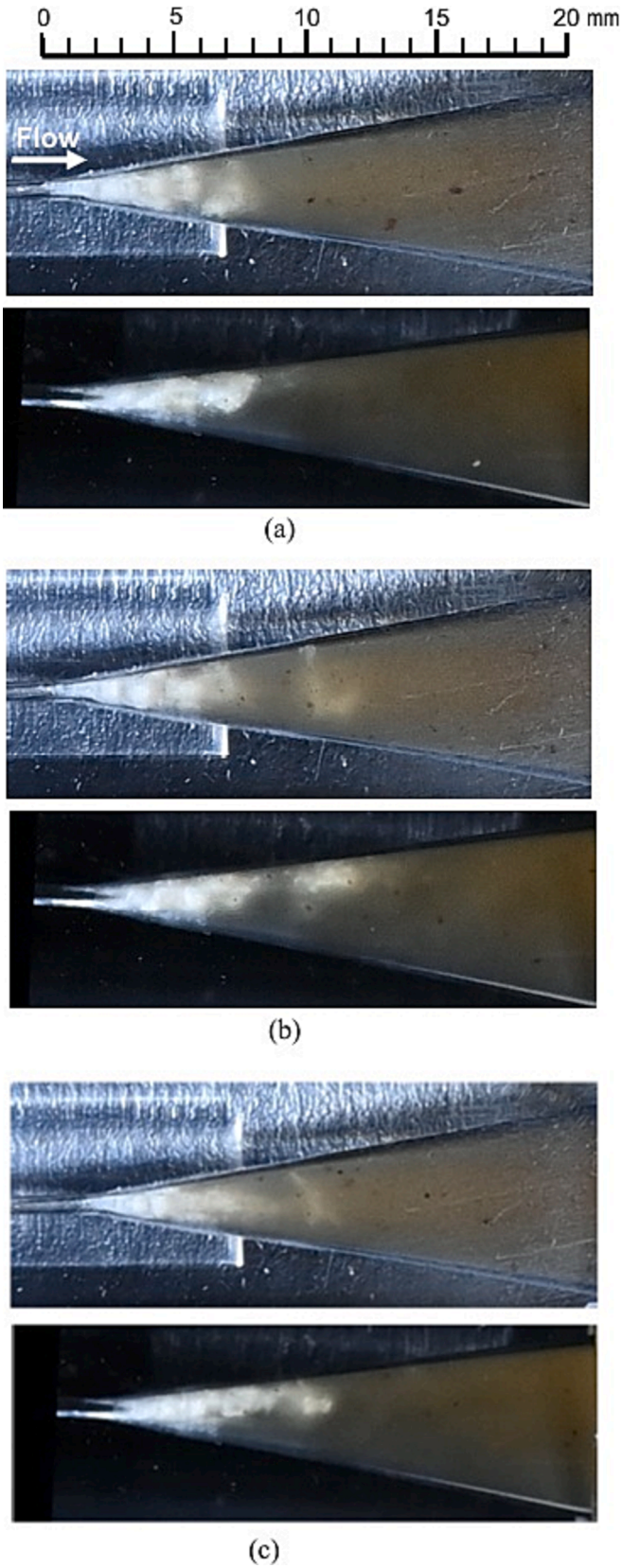

Fig. 9. Visualization of vortex cavitation with coffee grounds observed from two perspectives in a 30 vol% ethanol aqueous solution (p_1 = 3.4 MPa, p_2 = 0.28 MPa).

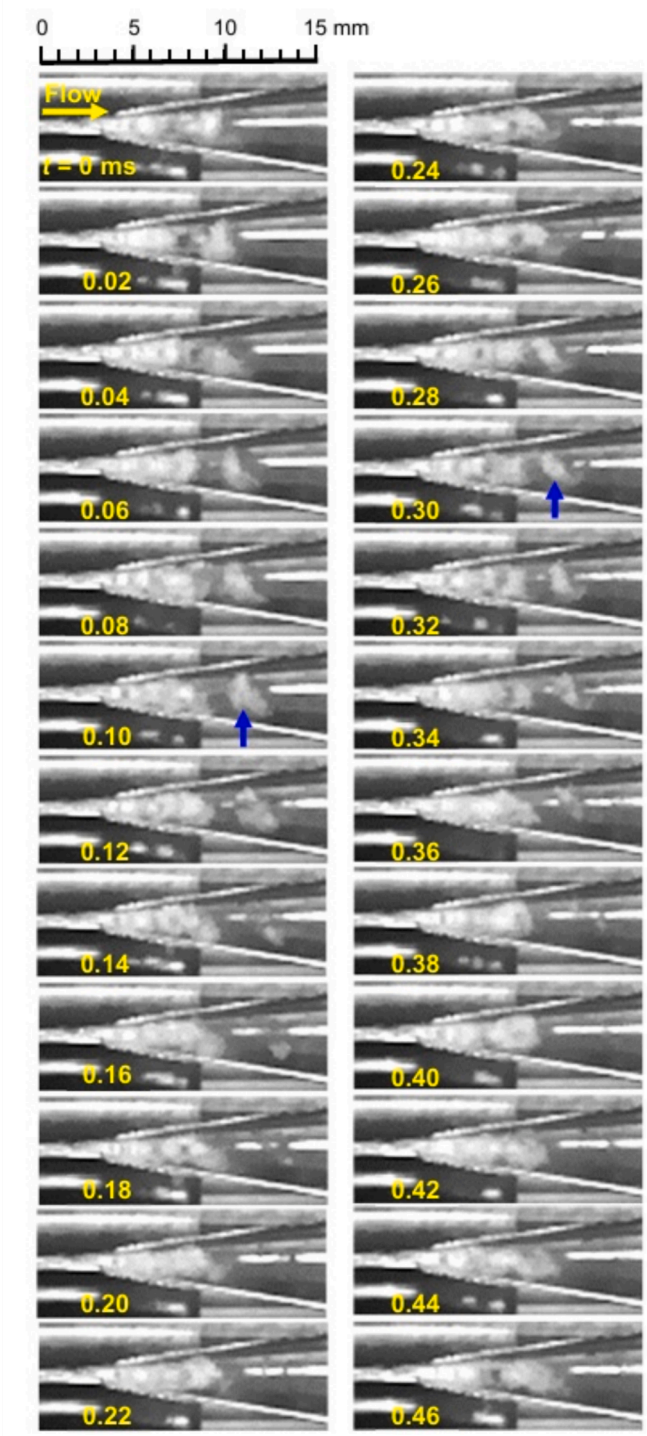

Fig. 10. Vortex cavitation observed by high-speed video camera in a 30 vol% ethanol aqueous solution ($p_1 = 3.4$ MPa, $p_2 = 0.28$ MPa).

a week. As depicted in Fig. 12, the double-cross sign is clearly visible in (a) the untreated solution with coffee grounds, and (b) the solution post-control process. However, the sign is difficult to discern in (c) following the cavitation process, suggesting that cellulose microfibrils remained suspended in the solution in the cavitation case after 150 min.

To compare the microfibrils produced with untreated coffee grounds, Fig. 13 displays: (a) untreated coffee grounds, (b) coffee grounds treated by the control process for 150 min, and (c) coffee grounds treated by cavitation for 150 min. For cases (b) and (c), after each respective process, coffee grounds were retrieved from the clear layer above the

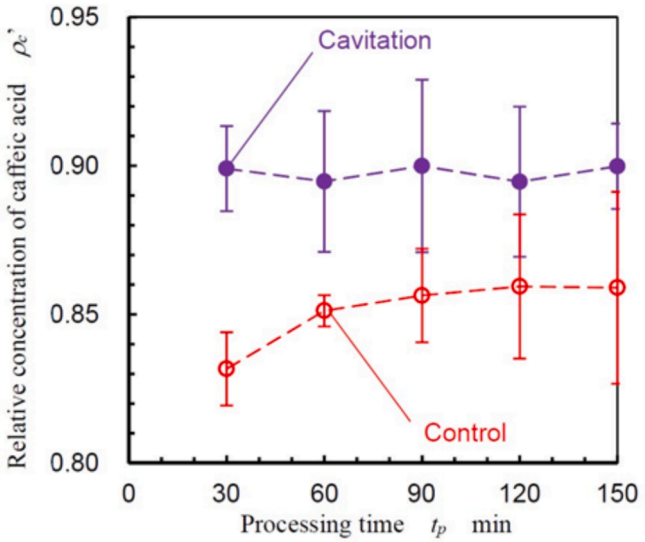

Fig. 11. Variation of caffeic acid concentration as a function of processing time in a 30 vol% ethanol aqueous solution.

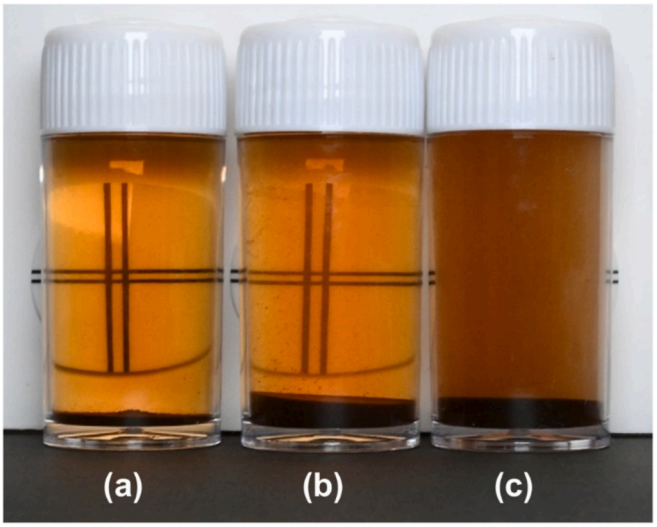

Fig. 12. Visual comparison of a 30 vol% ethanol aqueous solution: (a) without processing, (b) after the control process for 150 min, (c) after the cavitation process for 150 min.

sediment and then freeze-dried. Specifically in case (c), the yellow rectangular area is enlarged in (d) to highlight details. In Fig. 13 (d), the diameters of several microfibrils are marked with blue annotations.

As depicted in Fig. 13 (a), the size of the untreated coffee grounds ranges from tens to hundreds of micrometers after being crushed and screened using a wire mesh. Fig. 13 (b) shows that the coffee grounds, though smaller than those in (a), still range from tens to hundreds of micrometers. In contrast, following the cavitation process, microfibrils ranging from submicrometers to several micrometers in diameter were produced, as shown in Fig. 13. The aspect ratio of these microfibrils exceeds 100, indicating that their length surpasses several hundred micrometers. Thus, it can be concluded that hydrodynamic cavitation in a Venturi tube under the conditions of $p_1 = 3.4$ MPa and $p_2 = 0.28$ MPa effectively transforms coffee grounds into microfibrils.

4. Conclusions

To develop a sustainable process for spent coffee grounds (SCGs),

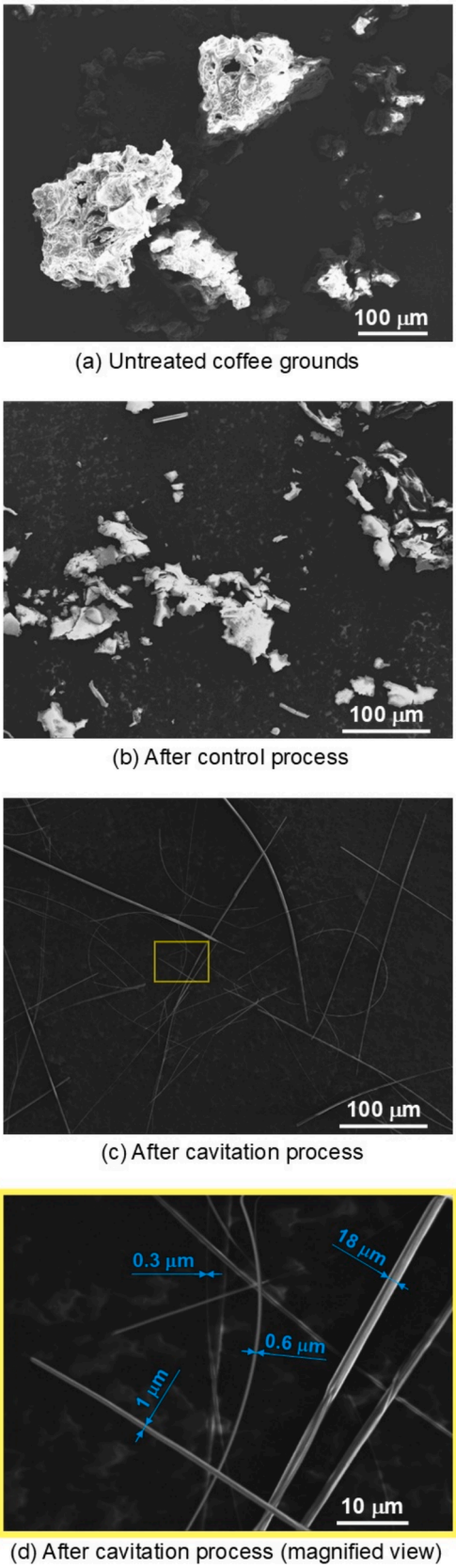

Fig. 13. Scanning Electron Microscope (SEM) images of coffee grounds and microfibrils.

this study explored the use of hydrodynamic cavitation in a Venturi tube to simultaneously extract caffeic acid and produce cellulose microfibrils. The experimental setup involved a Venturi tube with a throat diameter of 0.7 mm, where the upstream pressure (p_1) was maintained at 3.4 MPa. Unbrewed coffee grounds were chosen to ensure consistent results, as the ratio of caffeic acid in SCGs can vary with different brewing methods. The key findings from this study are summarized below:

1) Hydrodynamic cavitation, using a 30 vol% ethanol aqueous solution in the Venturi tube, effectively enhanced the extraction of caffeic acid from coffee grounds at $p_1 = 3.4$ MPa and a downstream pressure (p_2) of 0.28 MPa.
2) The process not only extracted caffeic acid but also simultaneously produced cellulose microfibrils.
3) The noise level of the cavitation, indicative of its aggressive intensity, peaked as a function of p_2 at a constant p_1. Optimizing p_2 significantly enhanced the aggressive intensity of hydrodynamic cavitation without additional energy input. Specifically, optimizing the downstream pressure p_2 of the Venturi tube reduced the electric power required for the pump by a factor of 20.
4) In experiments with a 30 vol% aqueous ethanol solution in the Venturi tube, a higher number of fine residual bubbles were observed at lower p_2 values. At higher p_2 values, these bubbles became less pronounced.
5) When hydrodynamic cavitation was performed with coffee grounds in a 30 vol% aqueous ethanol solution, vortex cavitation was clearly evident, similar to that observed with water. This vortex cavitation, inclined at a 45° angle to the main flow direction, was a component of the helical vortex.

These results demonstrate that hydrodynamic cavitation is a promising technique for valorizing spent coffee grounds by efficiently extracting valuable compounds and converting waste into useful byproducts.

CRediT authorship contribution statement

Hitoshi Soyama: Writing – original draft, Visualization, Resources, Project administration, Methodology, Investigation, Funding acquisition, Formal analysis, Data curation, Conceptualization. **Kousuke Hiromori:** Writing – review & editing, Methodology, Investigation, Formal analysis, Data curation. **Naomi Shibasaki-Kitakawa:** Writing – review & editing, Supervision, Methodology, Conceptualization.

Declaration of competing interest

The authors declare that they have no known competing financial interests or personal relationships that could have appeared to influence the work reported in this paper.

Acknowledgments

The research was partly supported by JSPS KAKENHI (22KK0050 and 23K25988) and Japan Science and Technology Agency (JST) CREST (JPMJCR2335).

Appendix A. . Luminescence intensity changing with the concentration ratio of ethanol

Fig. A1 displays the luminescence intensity caused by hydrodynamic cavitation in a Venturi tube as a function of the downstream pressure (p_2). The experimental setup and procedures align with those described in a previous study[99]. Luminescence intensity (I_L) measurements were taken at ethanol concentrations (C_e) of 0, 10, 20, 30, 40, and 50 vol

%. According to the "*Materials*" section 2.1, the injection pressure, also known as the upstream pressure of the Venturi tube, was set at 0.5 MPa. The I_L at C_e values of 0, 10, 20, 30, 40, and 50 vol% each showed a peak in relation to p_2. In Fig. A1, I_L was normalized to the peak value at $C_e = 0$ vol%, representing water, denoted as I_L. Fig. A2 illustrates the maximum luminescence intensity (I_{Lmax}) for each C_e, indicating that I_{Lmax} peaks at $C_e = 30$ vol %. Notably, the I_L of $C_e = 30$ vol% reached its maximum at $p_2 = 0.14$ MPa, and I_{Lmax} of $C_e = 30$ vol% was 2.1 times greater than that of water ($C_e = 0$ vol %.

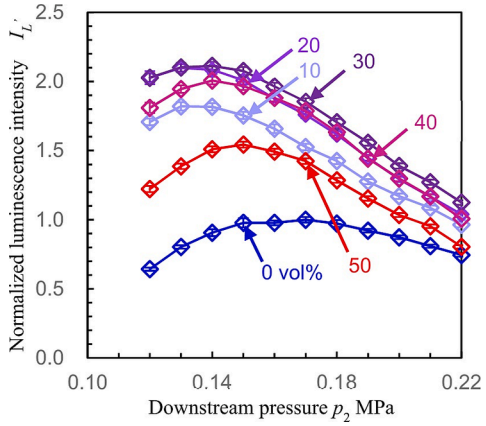

Fig. A1. Luminescence intensity from hydrodynamic cavitation in the Venturi tube as a function of downstream pressure p_2 across varying ethanol concentrations.

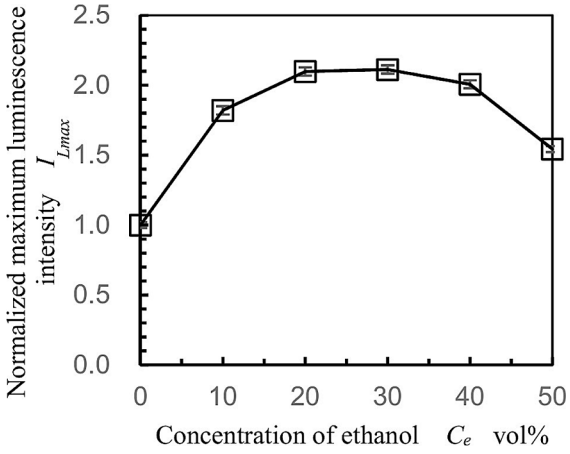

Fig. A2. Maximum luminescence intensity from hydrodynamic cavitation in the Venturi tube across ethanol concentration gradients.

Appendix B. . Cavitation erosion rate changing with the concentration ratio of ethanol

To explore the aggressive intensity of hydrodynamic cavitation under relatively high injection pressures, Fig. B1 depicts the change in mass loss over erosion time when exposed to a cavitating jet, using an ASTM G134 apparatus [101]. A cavitating jet, a type of hydrodynamic cavitation, is a submerged high-speed water jet that induces cavitation around itself. When materials are exposed to this jet, they experience mass loss due to cavitation. The cumulative erosion rate (*CER*) was defined as the mass loss divided by the erosion time, and the *CER* reached a maximum (CER_{max}) at a specific erosion time [101]. Higher aggressive intensities of the cavitating jet correlated with higher CER_{max}. A cavitation erosion test was employed to assess the aggressive intensity of the hydrodynamic cavitation. In this test, the injection pressure was set at 10 MPa, and the cavitation number (σ) was selected as 0.01485, as the peak aggressive intensity of the cavitating jet occurred at $\sigma \approx 0.014$. Copper was used as the test material, and the liquid temperature was maintained at 303 K. As depicted in Fig. B1, the mass loss (Δm) increases with erosion time (t_e). For a solution of 100 vol% ethanol, the slope of Δm versus t_e was notably less steep compared to that for water (0 vol% ethanol). However, the slopes at ethanol concentrations of 10, 30, and 50 vol% were steeper than those for water. Fig. B2 demonstrates the variation of CER_{max} with C_e, showing a maximum at $C_e = 30$ vol%.

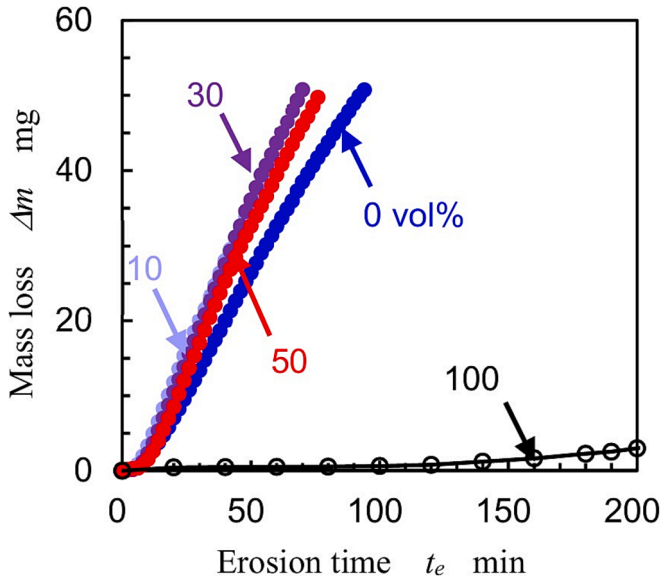

Fig. B1. Mass loss over time during exposure to a cavitating jet, as per ASTM G134 apparatus.

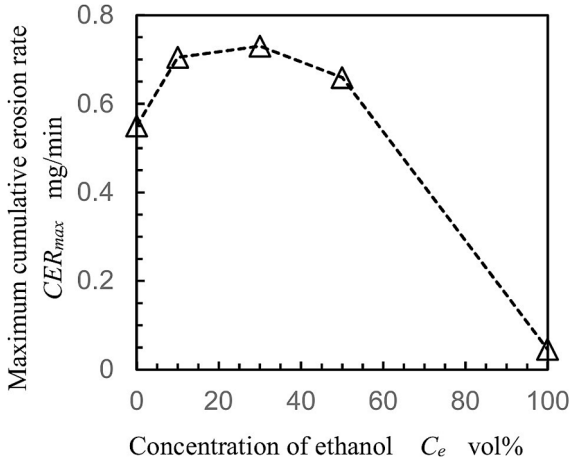

Fig. B2. Maximum cumulative erosion rate ($CER_{\max}$) across varying concentrations of ethanol.

Appendix C. . Effect of flow rate

In order to reveal the effect of flow rate Q on present cavitating flow through the Venturi tube, Fig. C1 illustrate Q changing with p_2 for 30 vol% ethanol aqueous solution and water. Fig. C2 shows the flow coefficient c_f as a function of p_2 (Fig. C2 (a)) and σ (Fig. C2 (b)). When p_2 was changed at constant p_1, Q was approximately equivalent as shown in Fig. C1. As expected, c_f at lower p_2 was slightly smaller than c_f at higher p_2 as shown in Fig. C2 (a), as cavitating region was developed as shown in Fig. 7. The relationship between p_2 and c_f differs for each p_1. On the other hand, the relationship between σ and c_f of 30 vol% ethanol aqueous solution is almost on the same line as shown in Fig. C2 (b), even if p_1 is different. Namely, the key parameter of the decrease of c_f was σ. As an example, Table C1 shows p_1, p_2, Δp, Q, σ, c_f, N_L and I_{cav}' for conditions A and B. Condition A corresponds to lower p_2 condition and condition B corresponds to $p_{2\ \max}$ at which noise level N_L had a maximum as shown in Figs. 4 and 5. The Q was $Q_A = 1.895 \pm 0.010$ L/min for condition A and $Q_B = 1.890 \pm 0.004$ L/min for condition B. Thus, the ratio of flow rate Q_A / Q_B was 1.003 ± 0.006. Namely, Q at constat p_1 were approximately equivalent. On the other hand, c_f was 0.879 ± 0.005 for condition A and 0.910 ± 0.002 for condition B. Note that the decrease of c_f was not so large at present condition of the used Venturi tube. Thus, the pressure difference $\Delta p = p_1 - p_2$ at condition A, i.e., 3.36 MPa was larger than that at condition B, i.e., 3.12 MPa. This is why Q_A and Q_B were approximately equivalent. Then, it can be concluded that the effect of Q on N_L and I_{cav}' was negligible, as I_{cav}' at conditions B was 11.8 times larger than that at condition A.

Table C1
Effect of flow rate on noise level (30 vol% ethanol aqueous solution).

			Condition A	Condition B
Upstream pressure of the Venturi tube	p_1	[MPa]	3.4	3.4
Downstream pressure of the Venturi tube	p_2	[MPa]	0.04	0.28
Pressure difference	$\Delta p = p_1 - p_2$	[MPa]	3.36	3.12
Flow rate	Q	[L/min]	1.895 ± 0.010	1.890 ± 0.004
Ratio of flow rate	Q_A / Q_B	[–]	1.003 ± 0.006	
Cavitation number	σ	[–]	0.04	0.12
Flow coefficient	c_f	[–]	0.879 ± 0.005	0.910 ± 0.002
Noise level	N_L	[dB]	79.5 ± 0.7	90.3 ± 0.7
Normalized aggressive intensity of cavitation	I_{cav}'	[–]	2.82 ± 0.12	33.37 ± 0.40

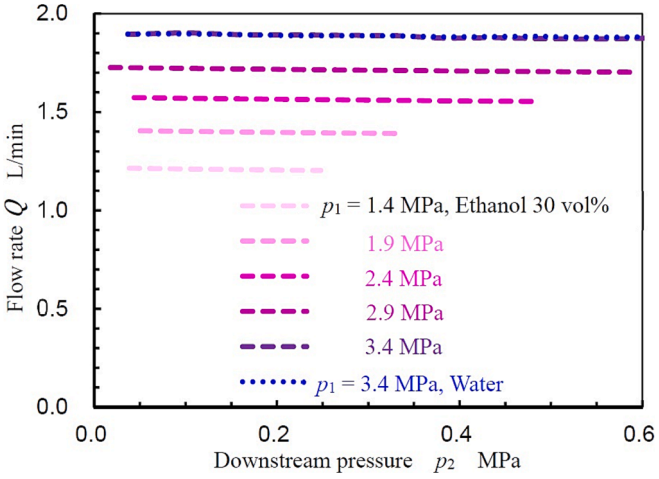

Fig. C1. Flow rate changing with downstream pressure

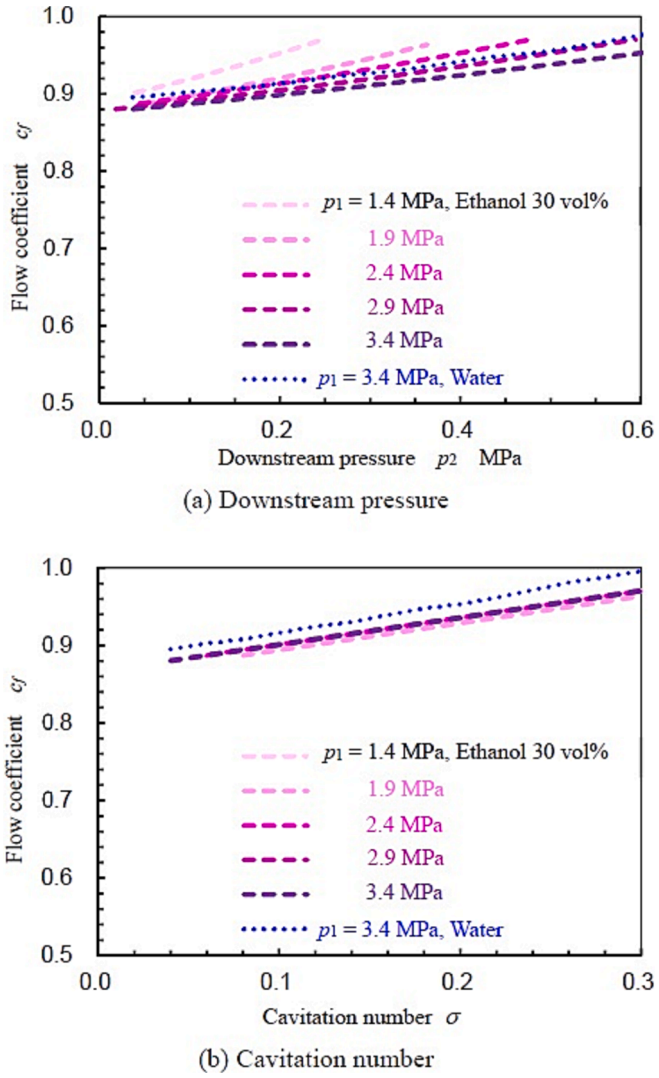

Fig. C2. Flow coefficient as a function of downstream pressure and cavitation number

Appendix D. . Comparison on size distribution between SEM observation and laser diffraction scattering method

In order to compare size distribution evaluated by a laser diffraction scattering method with SEM observation, Fig. D1 and Table D1 show the particle size distribution and diameters measured by a particle size analyzer (Beckman Coulter, Inc., Brea, CA, LS13 320) for untreated cellulose and the aqueous solution after hydrodynamic cavitation treatment. The sample was micro sized cellulose (Funacel II®, Funakoshi Co., Ltd, Tokyo, Japan). An aqueous solution containing 5 g of micro sized cellulose in 500 ml was treated hydrodynamic cavitation through Venturi tube at $p_1 = 3.1$ MPa for 10 h. Fig. D2 shows aspect of untreated cellulose and a sample obtained by freeze-drying an aqueous solution after the hydrodynamic cavitation treatment observed by SEM. As shown in Figs. D1 and D2, the hydrodynamic cavitation produces microfibrils from cellulose particles obviously. Regarding particle size distribution measured by the particle size analyzer, the particles size before treatment was 100 – 200 μm in diameter, and it became 100 – 200 nm in diameter by the treatment using the hydrodynamic cavitation. However, the SEM observations show that the diameter of the fine cellulose fibers after treatment was 10 – 20 nm. This is because the particle size analyzer assumed that the sample was spherical. Thus, at present experiment, SEM observation was chosen for the evaluation of fiber size.

Table D1
Diameter of samples measured by particle size analyzer.

	Untreated cellulose	After treatment
Average diameter	100.6 ± 58.3 μm	1.619 ± 5.289 μm
Median diameter	98.23 μm	0.184 μm
Mode diameter	153.8 μm	0.155 μm

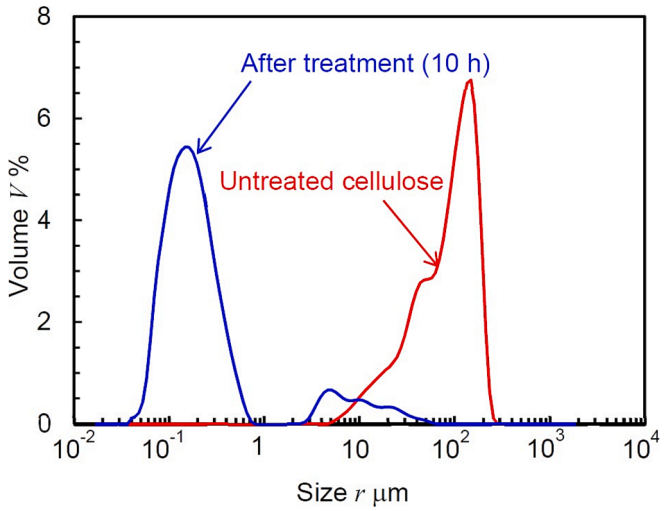

Fig. D1. Particle size distributions of samples measured by particle size analyzer

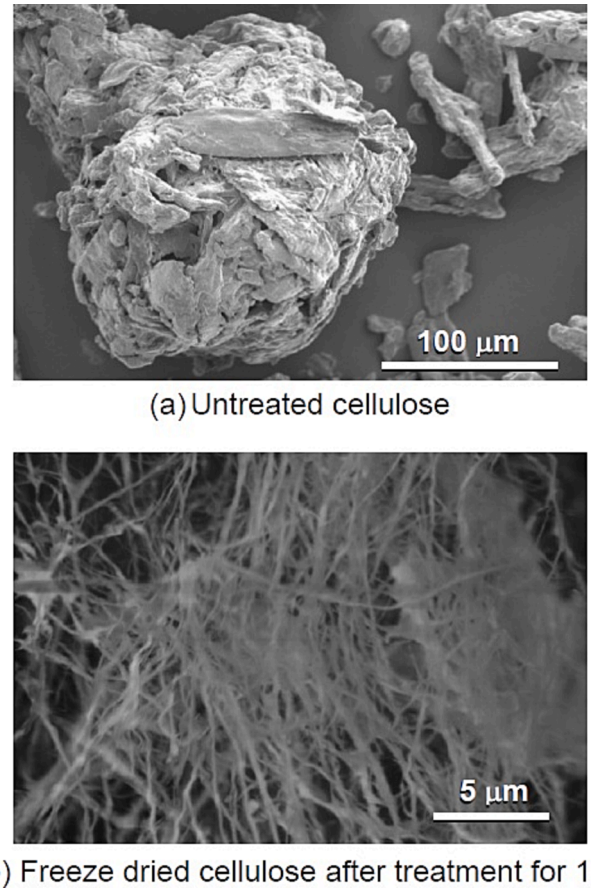

Fig. D2. SEM images of untreated cellulose and cellulose treated by hydrodynamic cavitation

Appendix E. . Production of cellulose microfibrils from coffee grounds without pulverization at high concentration ratio (23 %) using hydrodynamic cavitation

Fig. E1 shows a typical aspect of hydrodynamic cavitation arising in downstream of a ball valve, whose outer diameter of the ball was 12 mm and inner diameter of the hole in ball was 6.8 mm. The ball valve was used to generate cavitation, as the opening of the ball valve could be varied to avoid stacking due to large coffee grounds at the start of the process. The experimental setup was same as the present experiment which was shown in Fig. 1 except the Venturi tube. In Fig. E1, main flow direction was from left to right. The schematics of the ball valve was illustrated in Fig. E1. The upstream pressure was about 3 MPa. As the cavitating region generated by the ball valve was small, the downstream valve was opened. The opening of the ball

valve was controlled by the upstream pressure gauge and the pump's rotational speed to be equivalent to that of a Venturi tube with a 0.7 mm throat diameter. Fig. E2 reveals the aspect of cavitation arising in downstream of the ball valve observed by the high-speed video camera, whose recording speed was set at 40,000 fps. The typical vortex cavitation was indicated by the bule arrow in Fig. E2 at $t = 0.325$ ms. The ball valve can generate vortex cavitation which was observed in the Venturi tube. Namely, the hydrodynamic cavitation generated by the ball valve can be utilized for the production of cellulose microfibrils from coffee grounds without pulverization at high concentration ratio.

In order to demonstrate the production of cellulose microfibrils from coffee grounds without pulverization at high concentration ratio using hydrodynamic cavitation, Fig. E3 shows the SEM images of coffee grounds and microfibrils. 0.9 kg of the coffee grounds without pulverization were mixed into 3 L of the 30 vol% ethanol aqueous solution, and treated by the hydrodynamic cavitation arising in the ball valve for three hours. The concentration ratio of the coffee grounds was 23 %. The upstream pressure was about 3 MPa. The opening of the ball valve was controlled by the upstream pressure gauge and the pump's rotational speed to be equivalent to that of a Venturi tube with a 0.7 mm throat diameter as same as cavitation observation. As shown in Fig. E3 (b), the micro-meter order fiber was obtained from the coffee grounds without pulverization. Namely, the high concentration ratio such as 23 % of coffee grounds without pulverization can be processed by the hydrodynamic cavitation generated by the ball valve, and the microfibrils were obtained.

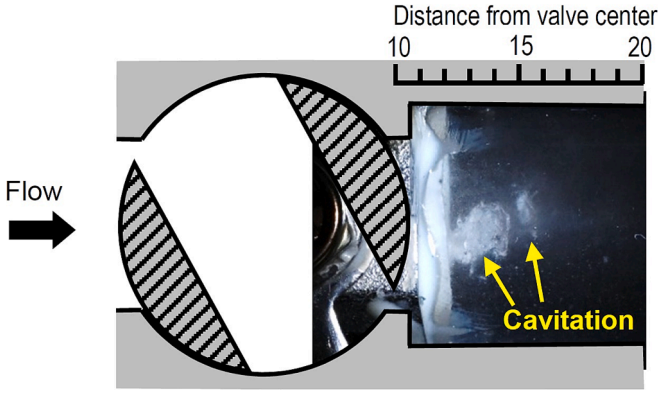

Fig. E1. Typical aspect of cavitation arising in downstream of ball valve (Water)

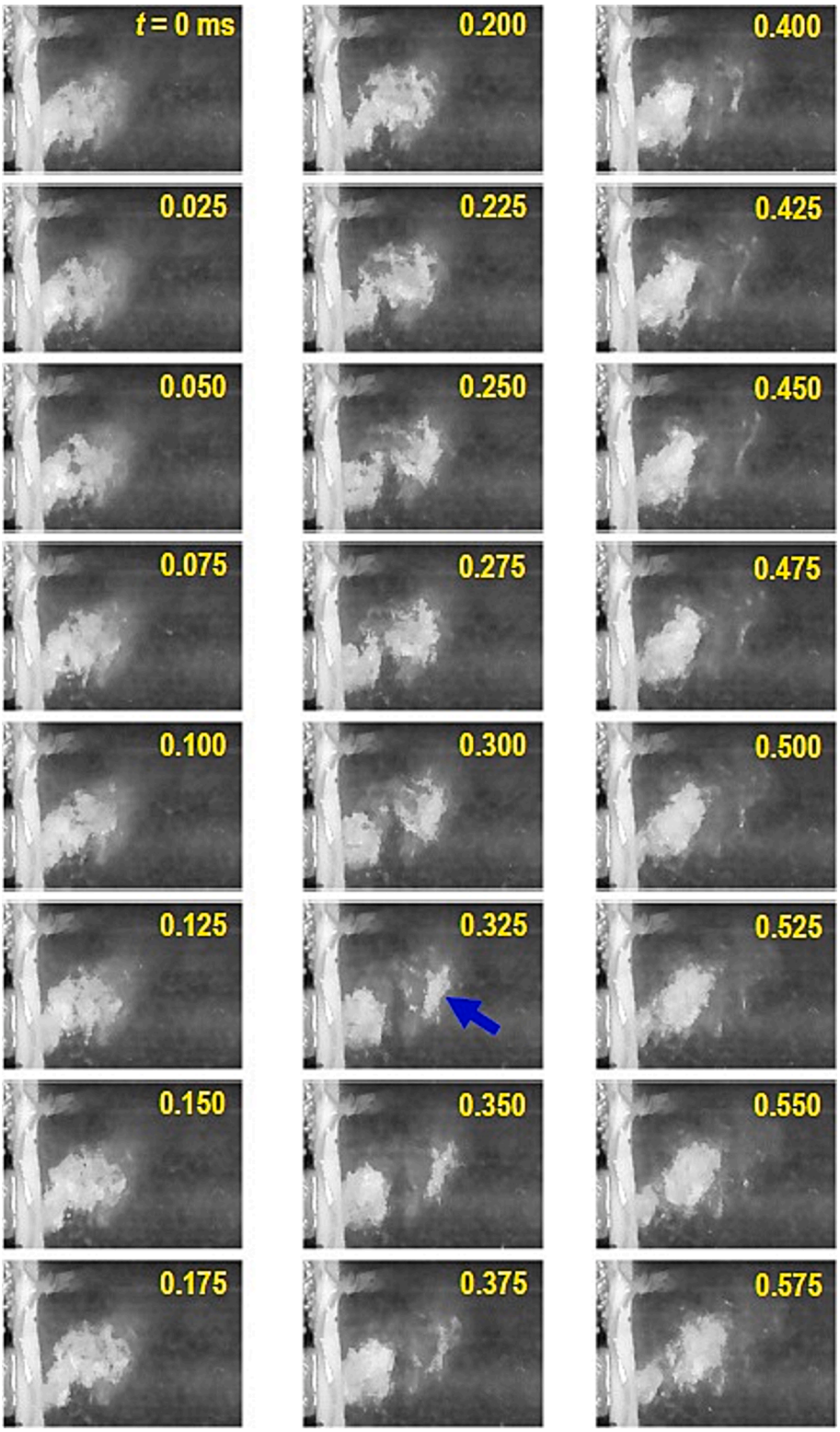

Fig. E2. Aspect of cavitation arising in downstream of ball valve changing with time (Water)

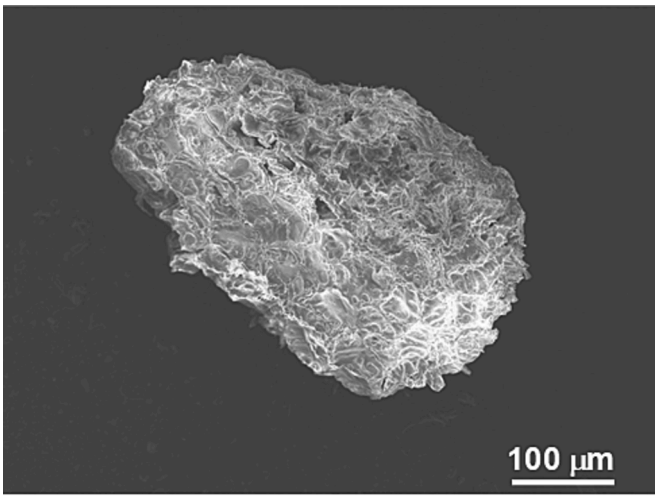

(a) Untreated coffee grounds without pulverization

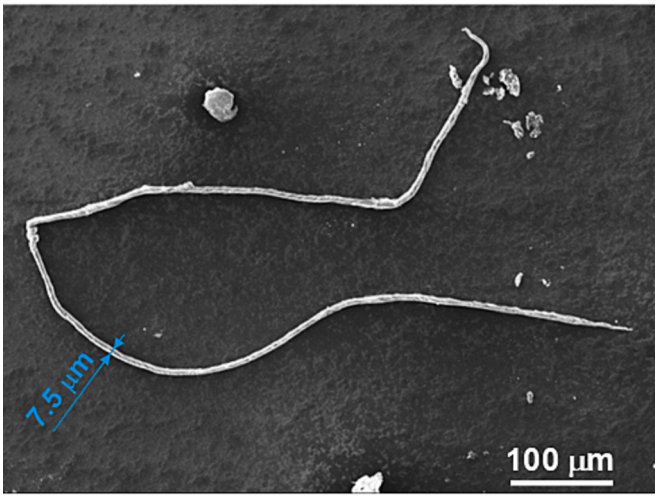

(b) After cavitation process

Fig. E3. Production of microfibril and sub-micro crystals by hydrodynamic cavitation arising in ball valve

References

[1] International Coffee Organization, Coffee report and outlook, (2023). https://icocoffee.org/documents/cy2022-23/Coffee_Report_and_Outlook_April_2023_-_ICO.pdf.

[2] V.P. Santos, P.C.C. Ribeiro, L.B. Rodrigues, Sustainability assessment of coffee production in Brazil, *Environ. Sci. Pollut. Res.* 30 (2023) 11099–11118, https://doi.org/10.1007/s11356-022-22922-z.

[3] N. Zhao, Z. Liu, T. Yu, F. Yan, Spent coffee grounds: Present and future of environmentally friendly applications on industries-a review, *Trends Food Sci. Technol.* 143 (2024), https://doi.org/10.1016/j.tifs.2023.104312.

[4] B. Yusufoğlu, G. Kezer, Y. Wang, Z.M. Ziora, T. Esatbeyoglu, Bio-recycling of spent coffee grounds: Recent advances and potential applications, *Curr. Opin. Food Sci.* 55 (2024), https://doi.org/10.1016/j.cofs.2023.101111.

[5] L.F. Ballesteros, M.J. Ramirez, C.E. Orrego, J.A. Teixeira, S.I. Mussatto, Optimization of autohydrolysis conditions to extract antioxidant phenolic compounds from spent coffee grounds, *J. Food Eng.* 199 (2017) 1–8, https://doi.org/10.1016/j.jfoodeng.2016.11.014.

[6] J.J. Rochin-Medina, K. Ramirez, J.G. Rangel-Peraza, Y.A. Bustos-Terrones, Increase of content and bioactivity of total phenolic compounds from spent coffee grounds through solid state fermentation by bacillus clausii, *J. Food Sci. Technol.* 55 (2018) 915–923, https://doi.org/10.1007/s13197-017-2998-5.

[7] A.F. Bondam, D. Diolinda da Silveira, J. Pozzada dos Santos, J.F. Hoffmann, Phenolic compounds from coffee by-products: Extraction and application in the food and pharmaceutical industries, *Trends Food Sci. Technol.* 123 (2022) 172–186, https://doi.org/10.1016/j.tifs.2022.03.013.

[8] M. Beaudor, P. Vauchel, D. Pradal, A. Aljawish, V. Phalip, Comparing the efficiency of extracting antioxidant polyphenols from spent coffee grounds using an innovative ultrasound-assisted extraction equipment versus conventional method, *Chemical Engineering and Processing - Process Intensification* 188, (2023), 10.1016/j.cep.2023.109358.

[9] F. Battista, E.M. Barampouti, S. Mai, D. Bolzonella, D. Malamis, K. Moustakas, M. Loizidou, Added-value molecules recovery and biofuels production from spent coffee grounds, *Renew. Sustain. Energy Rev.* 131 (2020), https://doi.org/10.1016/j.rser.2020.110007.

[10] A. Szaja, A. Montusiewicz, S. Pasieczna-Patkowska, E. Grządka, J. Montusiewicz, M. Lebiocka, Pre-treatment of spent coffee grounds using hydrodynamic cavitation, *Energies* 17 (2024), https://doi.org/10.3390/en17092229.

[11] M. Demestre, S.M. Messerli, N. Celli, M. Shahhossini, L. Kluwe, V. Mautner, H. Maruta, CAPE (caffeic acid phenethyl ester)-based propolis extract (Bio 30) suppresses the growth of human neurofibromatosis (NF) tumor xenografts in mice, *Phytotherapy Research* 23 (2009) 226–230, https://doi.org/10.1002/ptr.2594.

[12] J. Wu, C. Omene, J. Karkoszka, M. Bosland, J. Eckard, C.B. Klein, K. Frenkel, Caffeic acid phenethyl ester (CAPE), derived from a honeybee product propolis, exhibits a diversity of anti-tumor effects in pre-clinical models of human breast cancer, *Cancer Lett.* 308 (2011) 43–53, https://doi.org/10.1016/j.canlet.2011.04.012.

[13] C. Chen, Y.H. Kuo, C.C. Lin, C.Y. Chao, M.H. Pai, E.I. Chiang, F.Y. Tang, Decyl caffeic acid inhibits the proliferation of colorectal cancer cells in an autophagy-dependent manner in vitro and in vivo, *PLoS One* 15 (2020) e0232832, https://doi.org/10.1371/journal.pone.0232832.

[14] S. Mirzaei, M.H. Gholami, A. Zabolian, H. Saleki, M.V. Farahani, S. Hamzehlou, F. B. Far, S.O. Sharifzadeh, S. Samarghandian, H. Khan, A.R. Aref, M. Ashrafizadeh,

A. Zarrabi, G. Sethi, Caffeic acid and its derivatives as potential modulators of oncogenic molecular pathways: New hope in the fight against cancer, *Pharmacol. Res.* 171 (2021) 105759, https://doi.org/10.1016/j.phrs.2021.105759.
[15] M. Lukac, L. Slobodnikova, M. Mrva, A. Dusekova, M. Garajova, M. Kello, D. Sebova, M. Pisarcik, M. Kojnok, A. Vrtak, E. Kurin, S. Bittner Fialova, Caffeic acid phosphanium derivatives: Potential selective antitumor, antimicrobial and antiprotozoal agents, *Int. J. Mol. Sci.* 25 (2024) 1200, https://doi.org/10.3390/ijms25021200.
[16] N. Cortez, C. Villegas, V. Burgos, J.R. Cabrera-Pardo, L. Ortiz, I. Gonzalez-Chavarria, V.A. Nchiozem-Ngnitedem, C. Paz, Adjuvant properties of caffeic acid in cancer treatment, *Int. J. Mol. Sci.* 25 (2024) 7631, https://doi.org/10.3390/ijms25147631.
[17] F. Xing, N. Liu, C. Wang, X.D. Wang, Caffeic acid phenethyl ester promotes oxaliplatin sensitization in colon cancer by inhibiting autophagy, *Sci. Rep.* 14 (2024) 14624, https://doi.org/10.1038/s41598-024-65409-2.
[18] C.E. Brennen, Cavitation and bubble dynamics, Oxford University Press, 1995.
[19] K.S. Suslick, D.J. Flannigan, Inside a collapsing bubble: Sonoluminescence and the conditions during cavitation, *Annu. Rev. Phys. Chem.* 59 (2008) 659–683, https://doi.org/10.1146/annurev.physchem.59.032607.093739.
[20] H. Soyama, A.M. Korsunsky, A critical comparative review of cavitation peening and other surface peening methods, *J. Mater. Process. Technol.* 305 (2022) 117586, https://doi.org/10.1016/j.jmatprotec.2022.117586.
[21] H. Soyama, K.L. Wong, D. Eakins, A.M. Korsunsky, The effects of submerged laser peening, cavitation peening, and shot peening on the improvement of the torsional fatigue strength of powder bed fused Ti6Al4V produced through laser sintering, *Int. J. Fatigue* 185 (2024) 108348, https://doi.org/10.1016/j.ijfatigue.2024.108348.
[22] K.P. Varsha, S.-H. Yeo, H. Soyama, Investigation of surface finish and fatigue life of laser powder bed fused Ti-6Al-4V, *Int. J. Fatigue* 189 (2024) 108558, https://doi.org/10.1016/j.ijfatigue.2024.108558.
[23] D. Manoharan, M. Radhakrishnan, B.K. Tiwari, Cavitation technologies for extraction of high value ingredients from renewable biomass, *TrAC Trends Anal. Chem.* 174 (2024) 117682, https://doi.org/10.1016/j.trac.2024.117682.
[24] M. Gagol, A. Przyjazny, G. Boczkaj, Wastewater treatment by means of advanced oxidation processes based on cavitation - a review, *Chem. Eng. J.* 338 (2018) 599–627, https://doi.org/10.1016/j.cej.2018.01.049.
[25] P. Thanekar, P. Gogate, Application of hydrodynamic cavitation reactors for treatment of wastewater containing organic pollutants: Intensification using hybrid approaches, *Fluids* 3 (2018) 98, https://doi.org/10.3390/fluids3040098.
[26] B. Wang, Y. Liu, H. Zhang, W. Shi, M. Xiong, C. Gao, M. Cui, Hydrodynamic cavitation and its application in water treatment combined with ozonation: A review, *J. Ind. Eng. Chem.* 114 (2022) 33–51, https://doi.org/10.1016/j.jiec.2022.07.031.
[27] Y. Chen, C. Yin, Y. Song, Application of hydrodynamic cavitation in the field of water treatment, *Chem. Pap.* 77 (2023) 3521–3546, https://doi.org/10.1007/s11696-023-02754-y.
[28] M.H. Dehghani, R.R. Karri, J.R. Koduru, S. Manickam, I. Tyagi, N.M. Mubarak, Suhas, Recent trends in the applications of sonochemical reactors as an advanced oxidation process for the remediation of microbial hazards associated with water and wastewater: A critical review, *Ultrason Sonochem* 94 (2023) 106302, https://doi.org/10.1016/j.ultsonch.2023.106302.
[29] M. Zupanc, G. Primc, M. Dular, M. Petkovsek, R. Roskar, R. Zaplotnik, J. Trontelj, Proof-of-concept for removing micropollutants through a combination of sub-atmospheric-pressure non-thermal plasma and hydrodynamic (super) cavitation, *Ultrason. Sonochem.* 111 (2024) 107110, https://doi.org/10.1016/j.ultsonch.2024.107110.
[30] R. Atayupanqui Dueñas, P. Pacheco Umpire, L. Monzón Martínez, C. Chambi Mamani, J. Montalvo Andia, Study of hydrodynamic cavitation applied for the selective removal of escherichia coli and daphnia sp. Present in the cultivation of microalgae in agro-industrial wastewater, *J. Appl. Phycol.* 36 (2024) 2477–2488, https://doi.org/10.1007/s10811-024-03294-y.
[31] S.S. Arya, P.R. More, M.R. Ladole, K. Pegu, A.B. Pandit, Non-thermal, energy efficient hydrodynamic cavitation for food processing, process intensification and extraction of natural bioactives: A review, *Ultrason. Sonochem.* 98 (2023) 106504, https://doi.org/10.1016/j.ultsonch.2023.106504.
[32] Z. Askarniya, X. Sun, Z. Wang, G. Boczkaj, Cavitation-based technologies for pretreatment and processing of food wastes: Major applications and mechanisms – a review, *Chem. Eng. J.* 454 (2023) 140388, https://doi.org/10.1016/j.cej.2022.140388.
[33] M. Sivakumar, A.B. Pandit, Wastewater treatment: A novel energy efficient hydrodynamic cavitational technique, *Ultrason. Sonochem.* 9 (2002) 123–131, https://doi.org/10.1016/s1350-4177(01)00122-5.
[34] P.N. Patil, S.D. Bote, P.R. Gogate, Degradation of imidacloprid using combined advanced oxidation processes based on hydrodynamic cavitation, *Ultrason. Sonochem.* 21 (2014) 1770–1777, https://doi.org/10.1016/j.ultsonch.2014.02.024.
[35] M. Deggelmann, J.A. Nopel, F. Rudiger, D. Paustian, P. Braeutigam, Hydrodynamic cavitation for micropollutant degradation in water - correlation of bisphenol a degradation with fluid mechanical properties, *Ultrason. Sonochem.* 83 (2022) 105950, https://doi.org/10.1016/j.ultsonch.2022.105950.
[36] H. Han, M. Chen, C. Sun, Y. Han, L. Xu, Y. Zhao, Synergistic enhancement in hydrodynamic cavitation combined with peroxymonosulfate fenton-like process for bpa degradation: New insights into the role of cavitation bubbles in regulation reaction pathway, *Water Res.* 268 (2025) 122666, https://doi.org/10.1016/j.watres.2024.122666.
[37] K. Odehnalova, P. Pribilova, E. Marsalkova, S. Zezulka, F. Pochyly, P. Rudolf, B. Marsalek, Hydrodynamic cavitation-enhanced activation of sodium percarbonate for estrogen removal, *Water Sci. Technol.* 88 (2023) 2905–2916, https://doi.org/10.2166/wst.2023.382.
[38] Y. Huaccallo-Aguilar, A. Kumar, M. Meier, A. Lerch, S.F. Reinecke, Efficient removal of succinic acid by continuous hydrodynamic cavitation combined with ozone and side influent injection, *J. Environ. Manage.* 370 (2024) 122795, https://doi.org/10.1016/j.jenvman.2024.122795.
[39] H. Sun, J. Qin, L. Yi, Y. Ruan, J. Wang, D. Fang, A new process for degradation of Auramine O dye and heat generation based on orifice plate hydrodynamic cavitation (HC): Parameter optimization and performance analyses, *Process Saf. Environ. Prot.* 161 (2022) 669–683, https://doi.org/10.1016/j.psep.2022.03.058.
[40] J.-A. Nöpel, J. Fröhlich, F. Rüdiger, Impact of outgassing on dye degradation in jet cavitation, *Chem. Eng. Sci.* 302 (2025) 120937, https://doi.org/10.1016/j.ces.2024.120937.
[41] Z. Feng, F. Wang, K. Zhu, Z. Wang, J. Ning, Degradation of ammonia nitrogen by an economic combined hydrodynamic cavitation method, *Environ. Sci. Pollut. Res.* 30 (2023) 72782–72792, https://doi.org/10.1007/s11356-023-27504-1.
[42] T.-P. Yuan, X.-H. Huang, Y. Hu, S.-M. Wang, Q.-Y. Tao, G.-L. Pang, Aquaculture net cleaning with cavitation improves biofouling removal, *Ocean Eng.* 285 (2023) 115241, https://doi.org/10.1016/j.oceaneng.2023.115241.
[43] D. Ghayal, A.B. Pandit, V.K. Rathod, Optimization of biodiesel production in a hydrodynamic cavitation reactor using used frying oil, *Ultrason. Sonochem.* 20 (2013) 322–328, https://doi.org/10.1016/j.ultsonch.2012.07.009.
[44] M. Alsaiari, A. Bokhari, L.F. Chuah, M. Mubashir, F.A. Harraz, A.I. Almohana, P. L. Show, M.K. Awasthi, M.A. Rizk, Synthesis of methyl esters from hippophae rhamnoides via pilot scale hydrodynamic cavitation intensification reactor, *Renew. Energy* 205 (2023) 238–247, https://doi.org/10.1016/j.renene.2023.01.072.
[45] C.A. Prado, M.L.S. Cunha, R. Terán-Hilares, G.L. Arruda, F.A.F. Antunes, B. Pereira, S.S. da Silva, J.C. Santos, Hydrodynamic cavitation–assisted oxidative pretreatment and sequential production of ethanol and xylitol as innovative approaches for sugarcane bagasse biorefineries, *Bioenergy Res.* 16 (2023) 2229–2241, https://doi.org/10.1007/s12155-022-10555-6.
[46] Q. Wu, H. Luo, H. Wang, Z. Liu, L. Zhang, Y. Li, X. Zou, X. Wang, Simultaneous hydrodynamic cavitation and nanosecond pulse discharge plasma enhanced by oxygen injection, *Ultrason. Sonochem.* 99 (2023) 106552, https://doi.org/10.1016/j.ultsonch.2023.106552.
[47] M. Zuo, H. Yu, D. Wang, L. Fan, Jet cavitation-enhanced hydration method for the preparation of magnesium hydroxide, *Chemical Engineering and Processing - Process Intensification* 205, (2024), 110003, 10.1016/j.cep.2024.110003.
[48] S. Nagarajan, V.V. Ranade, Pretreatment of milled and unchopped sugarcane bagasse with vortex based hydrodynamic cavitation for enhanced biogas production, *Bioresour. Technol.* 361 (2022) 127663, https://doi.org/10.1016/j.biortech.2022.127663.
[49] S.H. Gharat, P.R. Gogate, Cavitation assisted intensification of biogas production: A review, *Environ. Qual. Manag.* 34 (2024) e22231, https://doi.org/10.1002/tqem.22231.
[50] M.A. Kelkar, P.R. Gogate, A.B. Pandit, Intensification of esterification of acids for synthesis of biodiesel using acoustic and hydrodynamic cavitation, *Ultrason. Sonochem.* 15 (2008) 188–194, https://doi.org/10.1016/j.ultsonch.2007.04.003.
[51] M. Setyawan, A. Budiman, P. Mulyono, S. Sutijan, Optimum extraction of algae-oil from microalgae using hydrodynamic cavitation, *International Journal of Renewable Energy Research* 8 451–458 (2018) 10.20508/ijrer.v8i1.6887.g7320.
[52] B.H. Samani, M. Behruzian, G. Najafi, E. Fayyazi, B. Ghobadian, A. Behruzian, M. Mofijur, M. Mazlan, J. Yue, The rotor-stator type hydrodynamic cavitation reactor approach for enhanced biodiesel fuel production, *Fuel* 283 (2021) 118821, https://doi.org/10.1016/j.fuel.2020.118821.
[53] J. Dai, A. Abdulwahab, J. Selvaraj, M. Hasanuzzaman, A. Kedia, W. Fengli, A comprehensive techno-eco-environmental investigation of an efficient biodiesel generation procedure through hydrodynamic cavitation, *Therm. Sci. Eng. Prog.* 55 (2024) 102916, https://doi.org/10.1016/j.tsep.2024.102916.
[54] K. Zhang, J. Zheng, Y. Xu, Z. Liao, Y. Huang, L. Lu, Enhanced fabrication of size-controllable chitosan-genipin nanoparticles using orifice-induced hydrodynamic cavitation: Process optimization and performance evaluation, *Ultrason. Sonochem.* 106 (2024) 106899, https://doi.org/10.1016/j.ultsonch.2024.106899.
[55] K.E. Preece, N. Hooshyar, A.J. Krijgsman, P.J. Fryer, N.J. Zuidam, Intensification of protein extraction from soybean processing materials using hydrodynamic cavitation, *Innov. Food Sci. Emerg. Technol.* 41 (2017) 47–55, https://doi.org/10.1016/j.ifset.2017.01.002.
[56] A. Presentato, A. Scurria, L. Albanese, C. Lino, M. Sciortino, M. Pagliaro, F. Zabini, F. Meneguzzo, R. Alduina, D. Nuzzo, R. Ciriminna, Superior antibacterial activity of integral lemon pectin extracted via hydrodynamic cavitation, *Chemistry Open* 9 (2020) 628–630, https://doi.org/10.1002/open.202000076.
[57] R. Mittal, V.V. Ranade, Intensifying extraction of biomolecules from macroalgae using vortex based hydrodynamic cavitation device, *Ultrason. Sonochem.* 94 (2023) 106347, https://doi.org/10.1016/j.ultsonch.2023.106347.
[58] K. Nakashima, Y. Ebi, N. Shibasaki-Kitakawa, H. Soyama, T. Yonemoto, Hydrodynamic cavitation reactor for efficient pretreatment of lignocellulosic biomass, *Ind. Eng. Chem. Res.* 55 (2016) 1866–1871, https://doi.org/10.1021/acs.iecr.5b04375.
[59] R. Teran Hilares, G.F. de Almeida, M.A. Ahmed, F.A.F. Antunes, S.S. da Silva, J. I. Han, J.C.D. Santos, Hydrodynamic cavitation as an efficient pretreatment method for lignocellulosic biomass: A parametric study, *Bioresour. Technol.* 235 (2017) 301–308, https://doi.org/10.1016/j.biortech.2017.03.125.

[60] M.J. Madison, G. Coward-Kelly, C. Liang, M.N. Karim, M. Falls, M.T. Holtzapple, Mechanical pretreatment of biomass - Part I: Acoustic and hydrodynamic cavitation, *Biomass Bioenergy* 98 (2017) 135–141, https://doi.org/10.1016/j.biombioe.2017.01.007.

[61] R. Teran Hilares, D.V. Kamoei, M.A. Ahmed, S.S. da Silva, J.I. Han, J.C.D. Santos, A new approach for bioethanol production from sugarcane bagasse using hydrodynamic cavitation assisted-pretreatment and column reactors, *Ultrason. Sonochem.* 43 (2018) 219–226, https://doi.org/10.1016/j.ultsonch.2018.01.016.

[62] R.T. Hilares, R.M. Dionizio, C.A. Prado, M.A. Ahmed, S.S. da Silva, J.C. Santos, Pretreatment of sugarcane bagasse using hydrodynamic cavitation technology: Semi-continuous and continuous process, *Bioresour. Technol.* 290 (2019) 121777, https://doi.org/10.1016/j.biortech.2019.121777.

[63] Z.L. Wu, D.F. Ferreira, D. Crudo, V. Bosco, L. Stevanato, A. Costale, G. Cravotto, Plant and biomass extraction and valorisation under hydrodynamic cavitation, *Processes* 7 (2019) 965, https://doi.org/10.3390/pr7120965.

[64] T.A. Bimestre, J.A.M. Junior, C.A. Botura, E. Canettieri, C.E. Tuna, Theoretical modeling and experimental validation of hydrodynamic cavitation reactor with a Venturi tube for sugarcane bagasse pretreatment, *Bioresour. Technol.* 311 (2020) 123540, https://doi.org/10.1016/j.biortech.2020.123540.

[65] R.T. Hilares, R.M. Dionizio, S.S. Munoz, C.A. Prado, R. de Sousa, S.S. da Silva, J. C. Santos, Hydrodynamic cavitation-assisted continuous pre-treatment of sugarcane bagasse for ethanol production: Effects of geometric parameters of the cavitation device, *Ultrason. Sonochem.* 63 (2020) 104931, https://doi.org/10.1016/j.ultsonch.2019.104931.

[66] T.A. Bimestre, J.A.M. Junior, E.V. Canettieri, C.E. Tuna, Hydrodynamic cavitation for lignocellulosic biomass pretreatment: A review of recent developments and future perspectives, *Bioresources and Bioprocessing* 9 (2022) 7, https://doi.org/10.1186/s40643-022-00499-2.

[67] X. Sun, S. Liu, X. Zhang, Y. Tao, G. Boczkaj, J.Y. Yoon, X. Xuan, Recent advances in hydrodynamic cavitation-based pretreatments of lignocellulosic biomass for valorization, *Bioresour. Technol.* 345 (2022) 126251, https://doi.org/10.1016/j.biortech.2021.126251.

[68] K. Thangavelu, R. Desikan, S. Uthandi, Optimization of combined lime and hydrodynamic cavitation for pretreatment of corncob biomass using response surface methodology for lignin removal, *Biomass Convers. Biorefin.* 13 (2022) 14433–14445, https://doi.org/10.1007/s13399-022-02728-2.

[69] R. Hamidi, M. Damizia, P. De Filippis, D. Patrizi, N. Verdone, G. Vilardi, B. de Caprariis, Recent developments and future outlooks of hydrodynamic cavitation as an intensification technology for renewable biofuels production, *J. Environ. Chem. Eng.* 11 (2023) 110819, https://doi.org/10.1016/j.jece.2023.110819.

[70] C.A. Prado, M.L.S. Cunha, G.L. Arruda, M.M. Cruz-Santos, F.A.F. Antunes, V. P. Shibukawa, R. Teran-Hilares, S.S. da Silva, J.C. Santos, Hydrodynamic cavitation-assisted acid pretreatment and fed-batch simultaneous saccharification and co-fermentation for ethanol production from sugarcane bagasse using immobilized cells of scheffersomyces parashehatae, *Bioresour. Technol.* 394 (2024) 130234, https://doi.org/10.1016/j.biortech.2023.130234.

[71] C.A. Prado, B.M.S. Loureiro, G.L. Arruda, J.C. Santos, A.K. Chandel, Hydrodynamic cavitation assisted pretreatment of sugarcane bagasse in the presence of yeast cell mass for the production of sugars and their use for biopigments production by monascus ruber, *Biomass Bioenergy* 190 (2024) 107434, https://doi.org/10.1016/j.biombioe.2024.107434.

[72] A. Di Fraia, S. Di Fraia, G.S. V, R. Banu J, N. Massarotti, Role of advanced oxidation processes in lignocellulose pretreatment towards biorefinery applications: A review on emerging trends and economic considerations, *Green Chemistry* 26, (2024), 8461-8496, 10.1039/d3gc05108k.

[73] L.A. Worku, R.K. Bachheti, A. Bachheti, T.S. Milessi, A.K. Chandel, Understanding the biochemical changes at molecular level during biomass pretreatment: A comprehensive analysis, *Cellul.* 31 (2024) 7281–7312, https://doi.org/10.1007/s10570-024-06081-7.

[74] A. Alemdar, M. Sain, Isolation and characterization of nanofibers from agricultural residues: Wheat straw and soy hulls, *Bioresour. Technol.* 99 (2008) 1664–1671, https://doi.org/10.1016/j.biortech.2007.04.029.

[75] N. Lavoine, I. Desloges, A. Dufresne, J. Bras, Microfibrillated cellulose - Its barrier properties and applications in cellulosic materials: A review, *Carbohydr. Polym.* 90 (2012) 735–764, https://doi.org/10.1016/j.carbpol.2012.05.026.

[76] R. Ciriminna, G.L. Petri, G. Angellotti, E. Fontananova, R. Luque, M. Pagliaro, Nanocellulose and microcrystalline cellulose from citrus processing waste: A review, *Int. J. Biol. Macromol.* 281 (2024) 135865, https://doi.org/10.1016/j.ijbiomac.2024.135865.

[77] K.-Y. Lee, Y. Aitomäki, L.A. Berglund, K. Oksman, A. Bismarck, On the use of nanocellulose as reinforcement in polymer matrix composites, *Compos. Sci. Technol.* 105 (2014) 15–27, https://doi.org/10.1016/j.compscitech.2014.08.032.

[78] R.A. Ilyas, M.R.M. Asyraf, L. Rajeshkumar, H. Awais, A. Siddique, K. Shaker, Y. Nawab, M.U. Wahit, A review of bio-based nanocellulose epoxy composites, *J. Environ. Chem. Eng.* 12 (2024) 113835, https://doi.org/10.1016/j.jece.2024.113835.

[79] W.T. Cao, F.F. Chen, Y.J. Zhu, Y.G. Zhang, Y.Y. Jiang, M.G. Ma, F. Chen, Binary strengthening and toughening of MXene/Cellulose nanofiber composite paper with nacre-inspired structure and superior electromagnetic interference shielding properties, *ACS Nano* 12 (2018) 4583–4593, https://doi.org/10.1021/acsnano.8b00997.

[80] P. Kumar, R.K. Deshmukh, S. Tripathi, K.K. Gaikwad, Review: Clay-based ethylene scavengers for sustainable active packaging applications, *J. Mater. Sci.* 59 (2024) 18338–18356, https://doi.org/10.1007/s10853-024-10258-7.

[81] Y. Qian, C. Wang, Y. Liu, B. Shi, J. Zhang, Y. Wei, G. Chen, Effects of plant source selection and chemi-mechanical treatment on the fiber microstructures and mechanical behaviors of nanocellulose films, *Wood Sci. Technol.* 59 (2024) 7, https://doi.org/10.1007/s00226-024-01613-7.

[82] R.R. Huerta, E.K. Silva, I. Ekaette, T. El-Bialy, M.D.A. Saldana, High-intensity ultrasound-assisted formation of cellulose nanofiber scaffold with low and high lignin content and their cytocompatibility with gingival fibroblast cells, *Ultrason. Sonochem.* 64 (2020) 104759, https://doi.org/10.1016/j.ultsonch.2019.104759.

[83] R.R. Huerta, E.K. Silva, T. El-Bialy, M.D.A. Saldana, Clove essential oil emulsion-filled cellulose nanofiber hydrogel produced by high-intensity ultrasound technology for tissue engineering applications, *Ultrason. Sonochem.* 64 (2020) 104845, https://doi.org/10.1016/j.ultsonch.2019.104845.

[84] H. Li, F. Cabanas-Gac, L. Hadidi, M. Bilodeau-Calame, A. Abid, K. Mameri, M. G. Rigamonti, S. Rousselot, M. Dolle, G.S. Patience, Ultrasound assisted wet media milling synthesis of nanofiber-cage $LiFePO_4$/C, *Ultrason. Sonochem.* 68 (2020) 105177, https://doi.org/10.1016/j.ultsonch.2020.105177.

[85] A. Ratnakumar, B.A.M.P. Samarasekara, S.D.A. Amarasinghe, L. Karunanayake, Effect of sonication time on cellulose nanofiber disintegration from locally available rice straw, *Macromol. Symp.* 402 (2022) 2100425, https://doi.org/10.1002/masy.202100425.

[86] M.M. Hassan, K. Saifullah, Ultrasound-assisted sustainable and energy efficient pre-treatments, dyeing, and finishing of textiles – A comprehensive review, *Sustain. Chem. Pharm.* 33 (2023) 101109, https://doi.org/10.1016/j.scp.2023.101109.

[87] M. Ghorbani, A.S. Aghdam, M.T. Gevari, A. Koşar, F.Ç. Cebeci, D. Grishenkov, A. J. Svagan, Facile hydrodynamic cavitation ON CHIP via cellulose nanofibers stabilized perfluorodroplets inside layer-by-layer assembled SLIPS surfaces, *Chem. Eng. J.* 382 (2020) 122809, https://doi.org/10.1016/j.cej.2019.122809.

[88] H. Zheng, Y. Zheng, J. Zhu, Recent developments in hydrodynamic cavitation reactors: Cavitation mechanism, reactor design, and applications, *Engineering* 19 (2022) 180–198, https://doi.org/10.1016/j.eng.2022.04.027.

[89] H. Soyama, Hydrogen produced by a cavitating jet, in: *7th International Conference on Advanced Oxidation Technologies for Water and Air Remediation* AOTs-7, 2001, pp. 128–129.

[90] A. Simpson, V.V. Ranade, Modeling hydrodynamic cavitation in Venturi: Influence of Venturi configuration on inception and extent of cavitation, *AIChE Journal* 65 (2019) 421–433, https://doi.org/10.1002/aic.16411.

[91] A. Simpson, V.V. Ranade, Modelling of hydrodynamic cavitation with orifice: Influence of different orifice designs, *Chem. Eng. Res. Des.* 136 (2018) 698–711, https://doi.org/10.1016/j.cherd.2018.06.014.

[92] L. Yi, J. Qin, H. Sun, Y. Ruan, L. Zhao, Y. Xiong, J. Wang, D. Fang, Improved hydrodynamic cavitation device with expanded orifice plate for effective chlorotetracycline degradation: Optimization of device and operation parameters, *Sep. Purif. Technol.* 280 (2022) 119840, https://doi.org/10.1016/j.seppur.2021.119840.

[93] J. Wang, H. Cheng, S. Xu, B. Ji, X. Long, Performance of cavitation flow and its induced noise of different jet pump cavitation reactors, *Ultrason. Sonochem.* 55 (2019) 322–331, https://doi.org/10.1016/j.ultsonch.2019.01.011.

[94] T. Chai, J. Wang, H. Cheng, Z. Zhang, X. Long, Experimental investigation of chocked cavitation flow and its oscillation mechanism in jet pump cavitation reactors under limited operation stage, *Exp. Therm Fluid Sci.* 161 (2025) 111332, https://doi.org/10.1016/j.expthermflusci.2024.111332.

[95] S. Nagarajan, V.V. Ranade, Pretreatment of lignocellulosic biomass using vortex-based devices for cavitation: Influence on biomethane potential, *Ind. Eng. Chem. Res.* 58 (2019) 15975–15988, https://doi.org/10.1021/acs.iecr.9b00859.

[96] A.H. Thaker, V.V. Ranade, Emulsions using a vortex-based cavitation device: Influence of number of passes, pressure drop, and device scale on droplet size distributions, *Ind. Eng. Chem. Res.* 62 (2023) 18837–18851, https://doi.org/10.1021/acs.iecr.2c03714.

[97] L. Liu, X. Yang, Y. Guo, B. Li, L.P. Wang, Reactive mixing performance for a nanoparticle precipitation in a swirling vortex flow reactor, *Ultrason. Sonochem.* 94 (2023) 106332, https://doi.org/10.1016/j.ultsonch.2023.106332.

[98] Y. Song, R. Hou, Z. Liu, J. Liu, W. Zhang, L. Zhang, Cavitation characteristics analysis of a novel rotor-radial groove hydrodynamic cavitation reactor, *Ultrason. Sonochem.* 86 (2022) 106028, https://doi.org/10.1016/j.ultsonch.2022.106028.

[99] H. Soyama, Luminescence intensity of vortex cavitation in a Venturi tube changing with cavitation number, *Ultrason. Sonochem.* 71 (2021) 105389, https://doi.org/10.1016/j.ultsonch.2020.105389.

[100] B. Jia, H. Soyama, Non-spherical cavitation bubbles: A review, *Fluids* 9 (2024) 249, https://doi.org/10.3390/fluids9110249.

[101] ASTM, G134-23, Standard test method for erosion of solid materials by a cavitating liquid jet, ASTM Standard 03 (02) (2023) 1–17.

[102] H. Soyama, J. Hoshino, Enhancing the aggressive intensity of hydrodynamic cavitation through a Venturi tube by increasing the pressure in the region where the bubbles collapse, *AIP Adv.* 6 (2016) 045113, https://doi.org/10.1063/1.4947572.

[103] C. Kang, H.X. Liu, H. Soyama, Estimation of aggressive intensity of a cavitating jet with multiple experimental methods, *Wear* 394 (2018) 176–186, https://doi.org/10.1016/j.wear.2017.11.001.

[104] H. Soyama, X. Liang, W. Yashiro, K. Kajiwara, E.M. Asimakopoulou, V. Bellucci, S. Birnsteinova, G. Giovanetti, C. Kim, H.J. Kirkwood, J.C.P. Koliyadu, R. Letrun, Y. Zhang, J. Ulicny, R. Bean, A.P. Mancuso, P. Villanueva-Perez, T. Sato, P. Vagovic, D. Eakins, A.M. Korsunsky, Revealing the origins of vortex cavitation in a venturi tube by high speed X-ray imaging, *Ultrason. Sonochem.* 101 (2023) 106715, https://doi.org/10.1016/j.ultsonch.2023.106715.